US Army Corps of Engineers
Construction Engineering Research Laboratories

USACERL Technical Report 98/99
July 1998

CONSTRUCTION PRODUCTIVITY ADVANCEMENT RESEARCH (CPAR) PROGRAM

Development and Demonstration of Advanced Design Composite Structural Components

by
Paul A. Howdyshell, Jonathan C. Trovillion,
Hota V.S. GangaRao, and Roberto Lopez-Anido

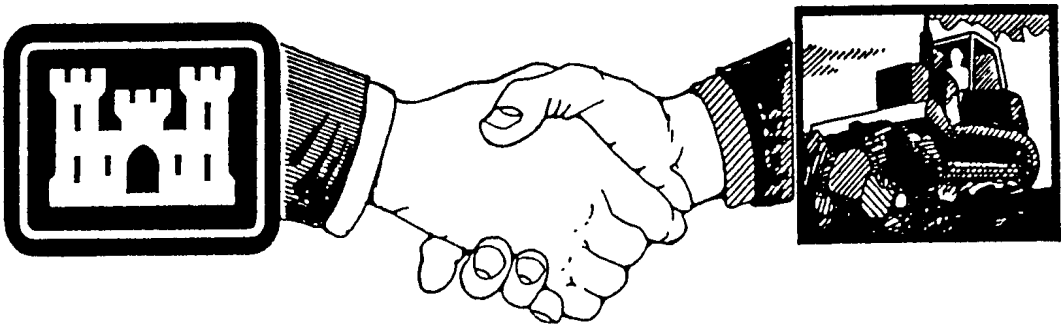

A Corps/Industry Partnership To Advance Construction Productivity and Reduce Costs

Foreword

This study was conducted for Headquarters, U.S. Army Corps of Engineers under the Construction Productivity Advancement Research (CPAR) Work Unit LV3, "Hybrid Advanced Design Composite Structural Elements." The technical monitors were J. Hartman (CECW-ED) and D. Chen (CEMP-ET).

The work was performed through a CPAR Cooperative Research and Development Agreement between the Maintenance Management and Preservation Division (FL-P) of the Facilities Technology Laboratory (FL), U.S. Army Construction Engineering Research Laboratories (USACERL) and West Virginia University – Constructed Facilities Center (WVU–CFC). Industry Partner Participants in this project were the Composites Institute (CI), a division of the Society of the Plastics Industry (SPI), and members of the Composites Institute Market Development Alliance (CI/MDA). The USACERL Principal Investigator was Dr. Paul A. Howdyshell and the WVU–CFC Principal Investigator was Dr. Hota V.S. GangaRao. Dr. Simon S. Kim is Chief, CECER-FL-P, and L. Michael Golish is Acting Operations Chief, CECER-FL. The USACERL technical editor was Gordon L. Cohen, Technical Information Team.

The member companies of the CI/MDA are gratefully acknowledged for providing the expertise and experience necessary to produce the new composite structural systems. Also gratefully recognized for their contributions are the design and field engineers from the participating consulting firms, the West Virginia Department of Highways, and the Federal Highway Administration of the U.S. Department of Transportation.

COL James A. Walter is the Commander of USACERL and Dr. Michael J. O'Connor is the Director.

Contents

List of Figures and Tables

Figures

Tables

1 Introduction

Background

Fiber-reinforced polymer (FRP) composites are created through the combination of two or more materials or constituents that differ in form or composition on a macro scale. The constituents retain their identities in the composite yet act in concert to perform a specific function more effectively than they could working independently. One principal constituent — the fiber — serves as the reinforcement and provides primary strength and stiffness in one direction. The other principal constituent — the polymer matrix — transfers stress between fibers to protect them from mechanical and environmental attack, and holds the reinforcement in the proper orientation to provide optimal material properties. A variety of synthetic fibers (glass, boron, carbon, and aramid) and polymer resins (thermoplastic/thermoset of a variety of chemical compositions) can be used to engineer specific properties for specific FRP composite applications in structural engineering. An FRP structural composite is identified as a matrix of polymeric materials that is reinforced by fibers or other reinforcing materials.* Normally, FRP composites are lightweight, high-strength, and have strong corrosion resistance. Some FRP composites, depending on the fiber selected and the fiber packing density, also have high stiffness and high fatigue resistance. For design purposes, composites are viewed macroscopically, as a statistically homogeneous anisotropic material.

Composites have been used for more than 50 years. Composite materials have been demonstrated to be effective in high-performance applications where traditional materials have failed, especially in aggressive environments. Currently, FRP composites are tracked in eight different market segments: transportation, construction, marine, business equipment, corrosion-resistant equipment, electrical, consumer products, and aircraft/aerospace. According to the Composites Institute, 1997 shipment of composites reached 3.42 billion lb.

* For additional details see *Introduction to Composites*, 3d ed. (Society of the Plastics Industry [SPI], Composites Institute, January 1995).

The construction market alone used nearly 700 million lb of composites, including such products as structural profiles, towers, buildings, panels, glazing, window lineals and doors, and bath tubs, just to name a few. Many applications in the corrosion-resistant equipment market (nearly 400 million lb) are load-bearing elements such as storage tanks, stacks, platforms, and piping used in such industries as chemical manufacturing, pulp and paper mills, petroleum, and gas extraction. However, the construction industry has mainly used composites in nonstructural applications, or in environments that are too aggressive chemically for more traditional building materials.

Several technical requirements have limited the use of FRP composites in the civil engineering market. To be attractive for use in civil engineering, FRP composites must:

- be competitive on a first-cost basis
- have a significant life-cycle cost advantage
- use design and construction procedures in accordance with traditional industry practices
- have a known and predictable life-cycle behavior.

Most FRP composite materials (resins, reinforcements, and related constituent materials) were developed for other end-use applications and are not optimized for civil engineering or construction applications. Optimization for civil engineering applications is further complicated because conventional civil engineering design procedures assume that most construction materials are homogeneous and isotropic, but FRP composites are highly anisotropic. Thus, conventional design procedures may not adequately define potential failure mechanisms, and they may not be effective or efficient in exploiting the directional strength and stiffness inherent in FRP composite systems.

Institutional constraints originate in the conservative makeup of the civil engineering industry, its inability to life-cycle test prototypes before commercialization, and its fear of liability associated with the use of new technology for which design and construction standards do not exist. Life-cycle structural performance and structural safety is the underlying institutional concern. Most engineered structures have a design life of 50 to 100 years but significant FRP composite applications only began appearing after World War II. Consequently, the ability to accurately project life-cycle behavior through accelerated testing and evaluation is very critical for FRP composites to gain widespread acceptance in the civil engineering structures market.

The Constructed Facilities Center at West Virginia University (WVU–CFC), with funding from the National Science Foundation (NSF), the Federal Highway Administration (FHWA), and the West Virginia Transportation Department had conducted several investigations into FRP composites for structural applications prior to the initiation of the effort described in this report. Based on their early findings, WVU–CFC submitted to the U.S. Army Corps of Engineers, through U.S. Army Construction Engineering Research Laboratories (USACERL), a Construction Productivity Advancement Research (CPAR) program proposal entitled "Development and Demonstration of Hybrid, Advanced-Design Composite Structural Elements." Their proposal was funded as part of the FY93 CPAR program with USACERL serving as the Corps partner on the program. The Constructed Facilities Center was joined by the SPI Composites Institute as the industrial partner. A Cooperative Research and Development Agreement (CRDA) between West Virginia University Research Corporation and USACERL was signed 10 January 1994 initiating the cooperative research effort. Amendments to the CPAR-CRDA were issued on 14 March 1994, 20 July 1994, and 24 March 1997. The CPAR-CRDA amendments clarified the U.S. Government liability, and changed the completion date from 31 December 1996, through 31 March 1997, to 30 September 1997.

Objective

The objective of this work as defined in the Research, Development and Commercialization Plan, Appendix A of the CPAR-CRDA, is as follows: "To develop, test, and demonstrate optimized, advanced-design composite structural components (beams, trusses, profile shapes, panels, etc.) for civil engineering applications. Material standards, specifications, and design protocol will be developed for these advanced composite components."

Approach

The project as planned by the CPAR-CRDA contains ten tasks spread over four phases. The organizations listed in parentheses after each task are the principal participants for that task.

Phase I

- Identify Applications and Required Structural Elements (CERL/WVU)
- Develop Theoretically Optimized Designs (CERL/WVU)

Phase II

- Fabricate Composite Structural Elements (WVU)
- Laboratory Testing of Fabricated Structures (CERL/WVU)
- Assessing Fastening/Connectivity Issues (CERL/WVU)

Phase III

- Optimization for Design and Manufacturing Processing (WVU)
- System Fabrication and Laboratory Testing (WVU)
- Construct Demonstration Facilities (CERL/WVU)

Phase IV

- Commercialization/Technology Transfer (CERL/WVU)
- Task J Final Technical Report (CERL/WVU)

The results of this research and demonstration are presented in three chapters:

- Fiber Architecture Optimization of Existing Pultruded Shapes
- Optimization of Shape, Fiber Architecture, and Fastening Systems
- Demonstration Projects.

2 Fiber Architecture Optimization of Existing Pultruded Shapes

Introduction

Pultrusion is the most cost-effective way to fabricate a structural composite with a constant cross-section and relatively uniform properties. The process consists of pulling fiber reinforcement material through a resin-impregnation bath and shaping die in which the resin is cured. Pultrusion is well suited for commercial production of composite structural elements because it:

- can be automated effectively
- is a continuous manufacturing process
- can produce members of unlimited length
- provides good production volume.

This research focused on pultruded structural component shapes already available through CPAR research participants. The goal of this phase of the research was to optimize fiber architecture with respect to specific loading applications. The work principally addressed structural members subjected to predominantly bending and shear loads (beams) and structural members subjected to predominantly axial loads (columns).

Theoretical Optimization

The objective of the optimizing existing shapes is to achieve the maximum safety factor for service conditions and for ultimate load per unit cost per specific loading application. This objective is achieved by maximizing stiffness and strength per unit weight. One of the advantages of composites is that mechanical properties can be tailored to specific applications by changing the fiber architecture of the reinforcement. Optimizing the fiber architecture also allows for consideration of mechanical issues that are relatively unique to composite material systems, such as shear deformations and shear-lag effects. Other considerations in the optimization of the fiber architectures are local buckling, lateral-torsional buckling, and torsional warping.

In general, the optimization of structural composite materials focuses on four major variables.

1. fiber architecture (fibers and resin)
2. structural application
3. cross-sectional shape characterization
4. fabrication process.

The fiber architecture variables include (1) the choice of fiber material, (2) the choice of matrix-binder material, (3) fiber volume fraction, and (4) fiber orientation.

Conventional E-glass was the fiber system used throughout this program. Glass fiber has the advantage of high strength at a cost significantly below most other fiber systems, and it has the highest potential of being cost-competitive with other traditional construction materials. It should be noted, however, that glass fibers have relatively low stiffness value as compared to both structural steel and carbon fibers. A thermosetting vinyl ester was selected as the matrix-binder material because it has low viscosity and it provides good corrosion protection and durability when cured. The fiber volume and orientation depend on whether the fibers are continuous, discontinuous, unidirectional, or multidirectional arrays. Traditional pultruded structural shapes are reinforced with unidirectional rovings (a group of untwisted parallel strands) and a minimum number of continuous strand mats (CSM) to enhance roving layers and provide transverse reinforcement. When conventional pultruded structural wide-flange (WF) shapes are tested, they normally fail by local compressive buckling of the flange, often followed by flange-web separation. This traditional fiber architecture is not optimal for carrying the compressive and tensile forces in the flange and the shear forces in the web.

Column applications involve predominantly axial loadings; beam applications involve predominantly flexural and shear loadings. Because these two loadings are significantly different, each will have its own optimal fiber architecture. The cross-sectional shape characterization in this work is restricted by the current size of pultrusion dies, which include many of the structural shapes common to traditional steel construction (WF, box, and circular pipe sections), but with limited sizes of the various shapes. Pultrusion is affected by several fabrication process variables, including:

- wetting
- degree of cure
- use of fabrics and mats

- fiber gathering (overlapping of mats).

A typical lay-up of any pultruded composite section contains roving layers and CSM layers (including off-angle-direction ply mats). The elastic stiffness properties of a section are determined based on the contribution of these three types of layers. While pultruded composite materials are not produced by laying up individual composite lamina, the composite cross-section does contain discrete layers, which allows application of classical micromechanical and macromechanical models. Elasticity solutions were used to obtain the micromechanical (stiffness) properties of each layer. Using these properties and classical lamination theory (see Jones 1975; Tsai and Hahn 1980), extension, bending, and coupling (ABBD) stiffness matrices for the section were computed, and flexural and axial stiffnesses determined for various fiber architectures.

The two commercially available sections (or existing dies) that were selected for fiber architecture optimization were a 12 in. x 12 in. x 1/2 in. wide-flange section and an 11 in. x 9 in. x 1/2 in. box section. These sizes represent the largest available pultrusion dies for the wide-flange and box shapes. Both shapes were optimized for structural beam loading—each with two fiber architectures—and the wide-flange shape was optimized for structural column loading with two fiber architectures. The proposed fiber architectures incorporated bidirectional knitted fabrics in addition to unidirectional rovings and CSM. It was assumed that 50 percent of the cross-section (by volume) is occupied by the fibers, and that the fiber volume fraction in the CSM layers and the angle ply layers is 30 percent. The proposed fiber lay-up and cross-sectional dimensions for the WF-FRP beam are shown in Figure 2.1*. Table 2.1 provides a detailed description of each fiber layer in the lay-up for the WF-FRP beam shown in Figure 2.1.

Optimized Shape Manufacturing

For experimental testing purposes, 500 ft of each of the two optimized WF-FRP beam fiber architectures and 500 ft of each of the two WF-FRP column fiber architectures were manufactured by Creative Pultrusions, Inc., of Alum Bank, PA. Due to problems coordinating with the CPAR partner participants in the project, the optimized fiber architectures for the box beams were not manufactured.

* Figures and tables are presented at the end of the first chapter in which they are discussed.

Experimental Testing of Optimized Shapes

Beam Testing

The WF-FRP beams with optimized fiber architectures were tested at WVU-CFC in three- and four-point bending about the strong and weak axes with a span length of (L) = 19 ft. The two optimized fiber architectures were tested in the "AC" series, incorporating bidirectional cross-ply fabrics (0/90 degrees) and angle-ply fabrics (±45 degrees); and the "A" series, incorporating bidirectional angle-ply fabrics (±45 degrees). Comparison tests were conducted on existing pultruded products. Maximum deflection load ratios (δ_m/P) were obtained by a linear regression analysis. Table 2.2 summarizes the results of the stiffness tests in terms of apparent modulus of elasticity (E_{app}). Bending stiffness is a function of the maximum deflection-load ratio (δ_m/P) and the shear bending deflection ratio (δ_{ms}/δ_{mb}) as follows:

$$(EI) = \frac{L^3}{48\left(\delta_m / P\right)}\left(1+\frac{\delta_{ms}}{\delta_{mb}}\right) = E_{app} I\left(1+\frac{\delta_{ms}}{\delta_{mb}}\right)$$

The apparent modulus of elasticity (E_{app}) and the beam cross-section moment of inertia (I) are introduced in the above equation. E_{app} varies with the ratio of δ_{ms}/δ_{mb}, and hence with the beam length, resulting in a smaller-than-actual value for the modulus of elasticity. But E_{app} is used as a reference value for design. The resulting sections showed increases in bending stiffness from 34 percent (strong axis, A series) to 53 percent (weak axis, AC series) as compared to existing pultruded products. (Bending tests on the existing product produced an $E_{app} \approx 2.8 \times 10^6$ psi.)

Column Testing

Local Buckling

Column specimens were received at USACERL from Creative Pultrusions, Inc., for laboratory testing. Two specimen types (F1 and F2) had optimized fiber architectures; these were 12 in. x 12 in. x 1/2 in. wide-flange columns. For comparison, stock specimens with the existing commercial fiber architecture also were tested for local buckling. The wide-flange columns have a width and depth *b = h = 304.8 mm (12 in)*, with both flanges and the web having thickness *t = 12.7 mm (½ in)*. The area of the cross-section for all specimens was *S=112.9 cm^2 (17.5 in^2)*. The difference between the optimized samples was the fiber reinforcement used: the F1 samples contain roving and CSM while the F2

samples contain additional stitched bidirectional fibers to achieve a higher local buckling load.

The samples were tested using an MTS 1 million lb closed-loop universal tension/compression testing machine. The samples were clamped at the ends by potting them into steel grooved end fixtures. The effect of these end fixtures was to introduce a fixed-end condition by restricting end rotation. The end fixtures rested on fixed flat plates. The loading rate for all tests was 0.05 in./min. The data measured from the experiments were the compressive applied load, the crosshead displacement of the machine, and the lateral deflections of the column flanges and webs along its length. The deflection measurements were taken using 15 linear variable differential transformers (LVDTs). Figure 2.2 depicts the overall test setup. To ensure that the LVDTs were not located at an inflection point on the specimen during testing, the lengths of the columns were chosen to correspond to 3 local buckling half waves while the LVDTs were located at the quarter-points along the length. Figure 2.3 shows the locations of the 15 LVDTs. The off-the-shelf specimens were 71 in. long, and both the F1 and F2 specimens were 59 in. long.

The objective of the data reduction schemes in the WVU analytical model is to determine the critical local buckling load and the curvature of the post-critical path of the column. Because the samples contain imperfections, non-zero lateral deflections are recorded for all values of the load, making it difficult to identify the critical local buckling load directly from the load-deflection plot (Figure 2.4). In the case of local buckling, the location of the maximum lateral deflection of the buckling mode is not known *a priori*, unlike the case of global buckling where the maximum deflection occurs at the mid-span. Therefore, the magnitude of the displacement recorded by the LVDTs depends on their location along the length of the column. Also, the load displacement data may reveal more or less deflection for a given load depending on the magnitude of the imperfections. It is therefore necessary to process the data to obtain a critical local buckling load and post-critical curvature independently from the magnitude of the imperfection and the position of the transducers.

Southwell's method, conceived for global buckling (Southwell 1941) was extended to the case of local buckling taking into account that the displacement transducers may not be placed at the point of maximum deflections of the buckling mode. The load deflection data are assumed to have a hyperbolic shape. By plotting the lateral deflection / load versus lateral deflection (Figure 2.5), a straight line is obtained and a linear regression can be done to find the slope and the abscissa at zero load. The inverse of the slope is the critical load, or asymptote of the load deflection curve. The abscissa at zero load gives an

indication of the imperfections in the sample (Tomblin and Barbero 1994). The average localized buckling strength of the two optimized fiber architectures were 37 and 63 percent higher than the buckling strength of the off-the-shelf FRP samples. A summary of the results of the testing is given in Table 2.3.

Compression Testing

Column specimens were received at USACRREL for laboratory testing. These specimens were the 12 in. x 12 in. x 1/2 in. WF-FRP columns with optimized fiber architectures for columns. A total of 17 F1 and 9 F2 specimens were cut to a length of 5 in. The specimens were instrumented with strain gages as shown in Figure 2.6. Initially, the intent of the testing was to determine the compressive modulus and the ultimate compressive strength for both fiber architectures. The specimens were potted in end grips (as in the local buckling tests) and tested in compression. An F2 specimen was tested to failure, with a maximum load of 820 kips (kilo pounds) and a failure stress of 47,278 pounds per square inch (psi). The testing machine was damaged as a result of the first test, so other specimens could not be tested to failure.

Six other specimens — 3 F1 and 3 F2 — were tested to determine the elastic modulus, both at room temperature and lower temperatures. These specimens were instrumented with six strain gages apiece. Two different test procedures were conducted on the six specimens. Table 2.4 gives a summary of the specimens and the tests conducted.

Compression tests using the Geokon test machine were conducted by increasing or decreasing the load in 40,000 lb increments and taking a strain reading at each increment. Compression tests using the MTS test machine were conducted at a loading/unloading rate of 60,000 lb/minute for three cycles. During testing, the specimens tended to barrel out, superimposing a bending strain as well as an axial compressive strain in the flange walls. To help counteract this effect, the readings of the inside and outside strain gages on one flange were averaged. The data was then plotted as stress versus average strain. A typical plot of stress versus average strain is shown in Figure 2.7. The specimens were tested at 23 °C, 0 °C, -20 °C, and –40 °C. The specimens tended to get somewhat stiffer as the temperature decreased. The secant modulus of elasticity at the 10 ksi stress level varied from 10,000 ksi at 23 °C to 12,200 ksi at –40 °C. A typical plot of stress versus average strain is shown in Figure 2.8.

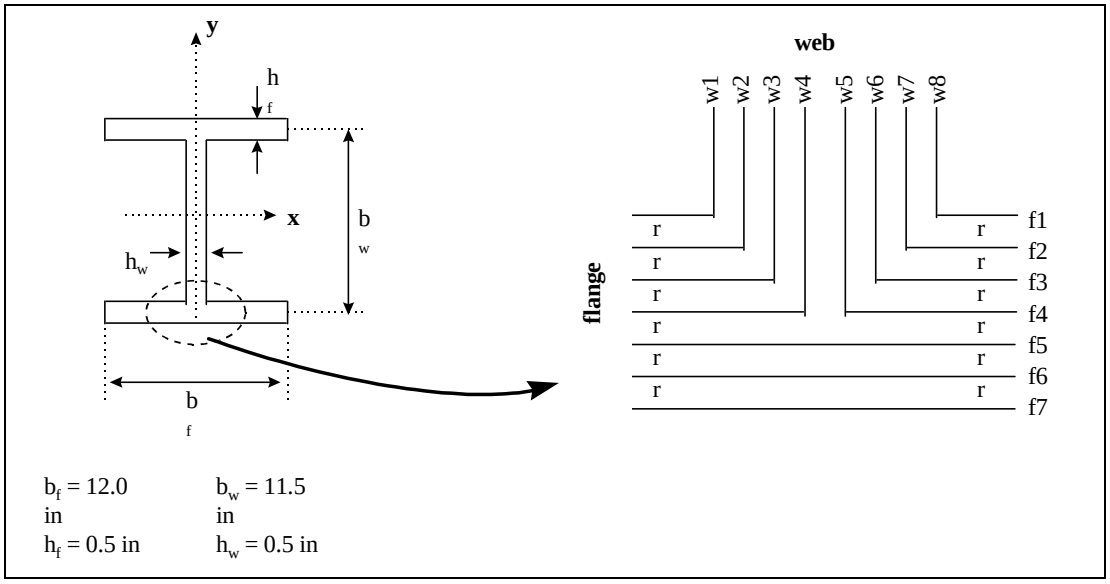

Figure 2.1. Cross-section dimensions and fiber lay-up for WF beams.

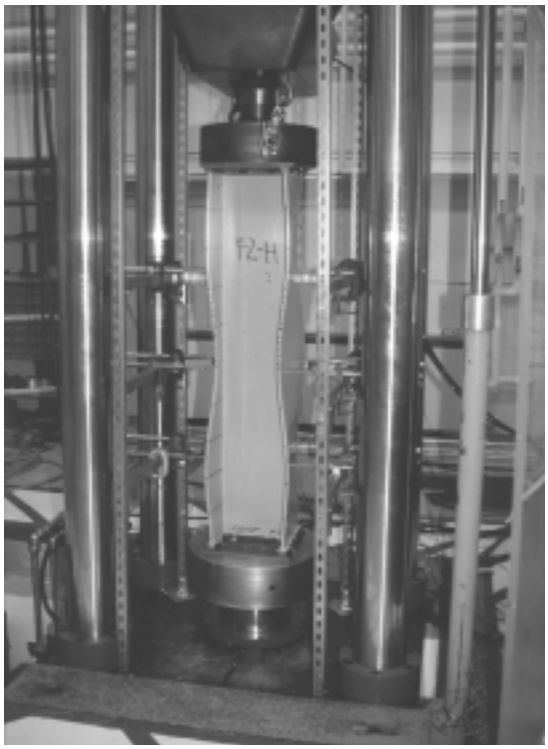

Figure 2.2. Setup for localized buckling test showing wave form of column flange under load.

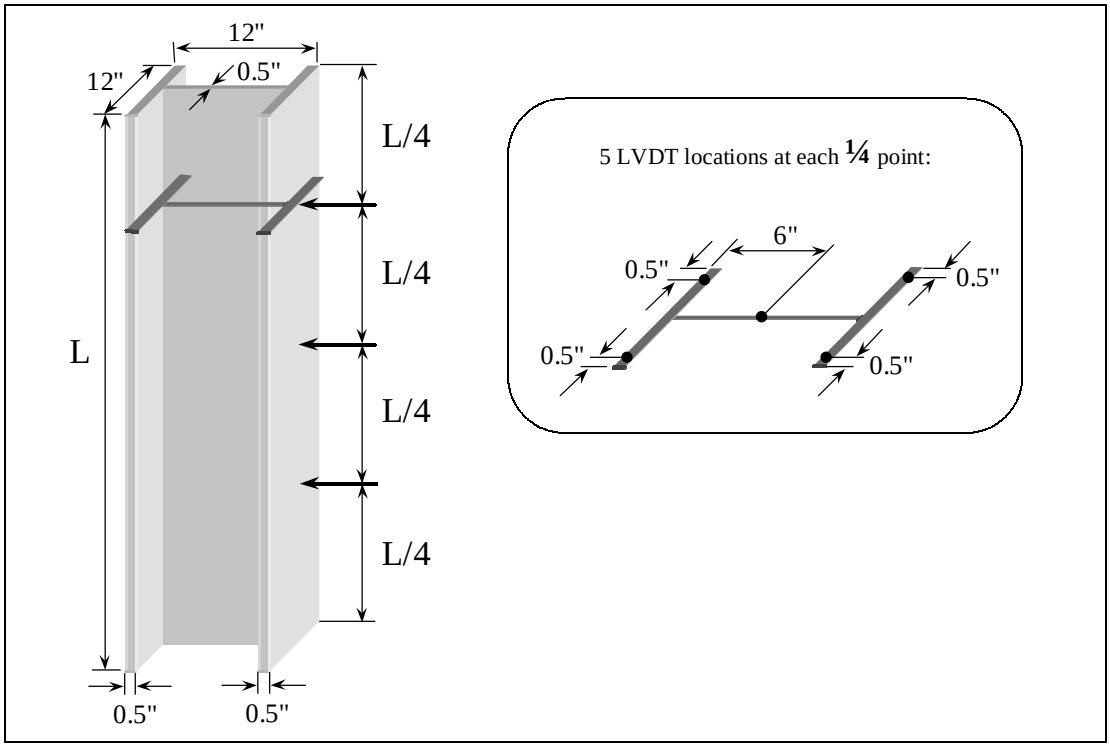

Figure 2.3. LVDT locations on column specimen.

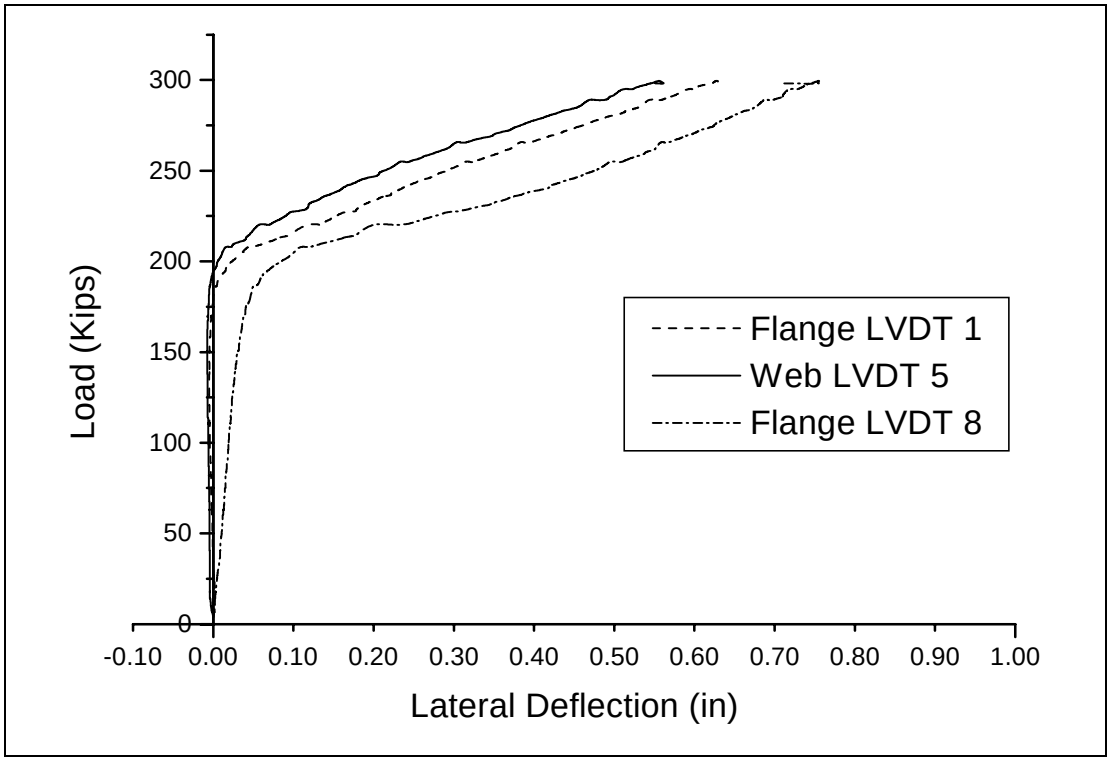

Figure 2.4. Load-deflection plots for local buckling tests of WF-FRP composite columns.

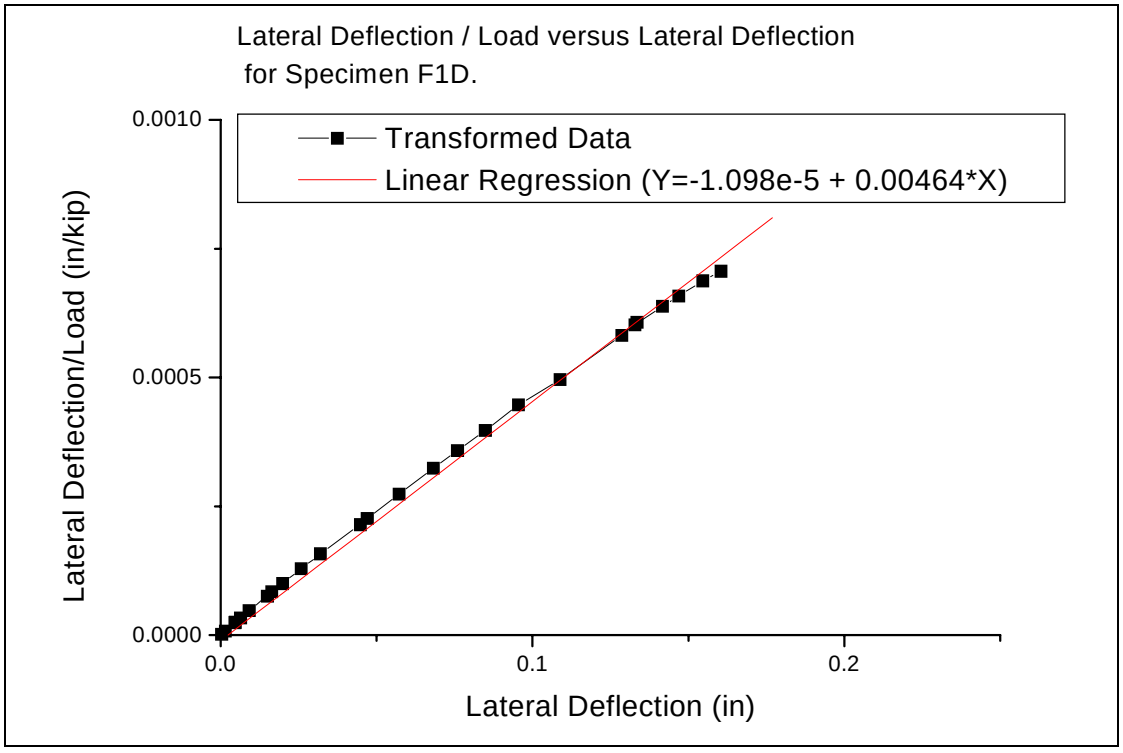

Figure 2.5. Linear regression plot of transformed data in load-deflection tests for local buckling of WF-FRP composite columns.

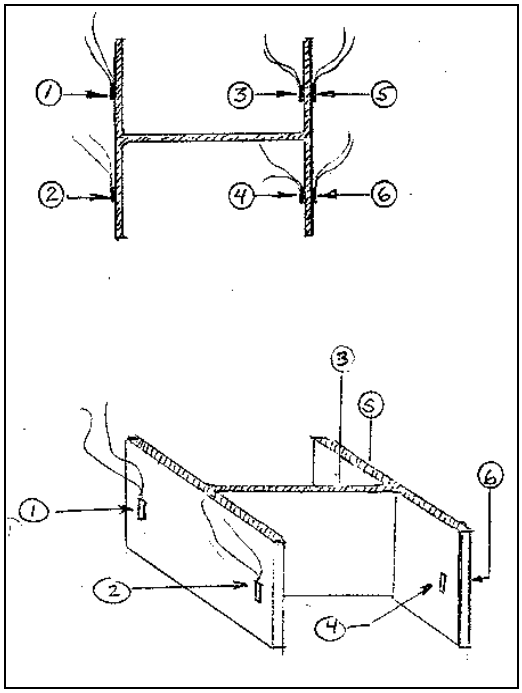

Figure 2.6. Strain gage layout for compression testing of WF-FRP composite columns.

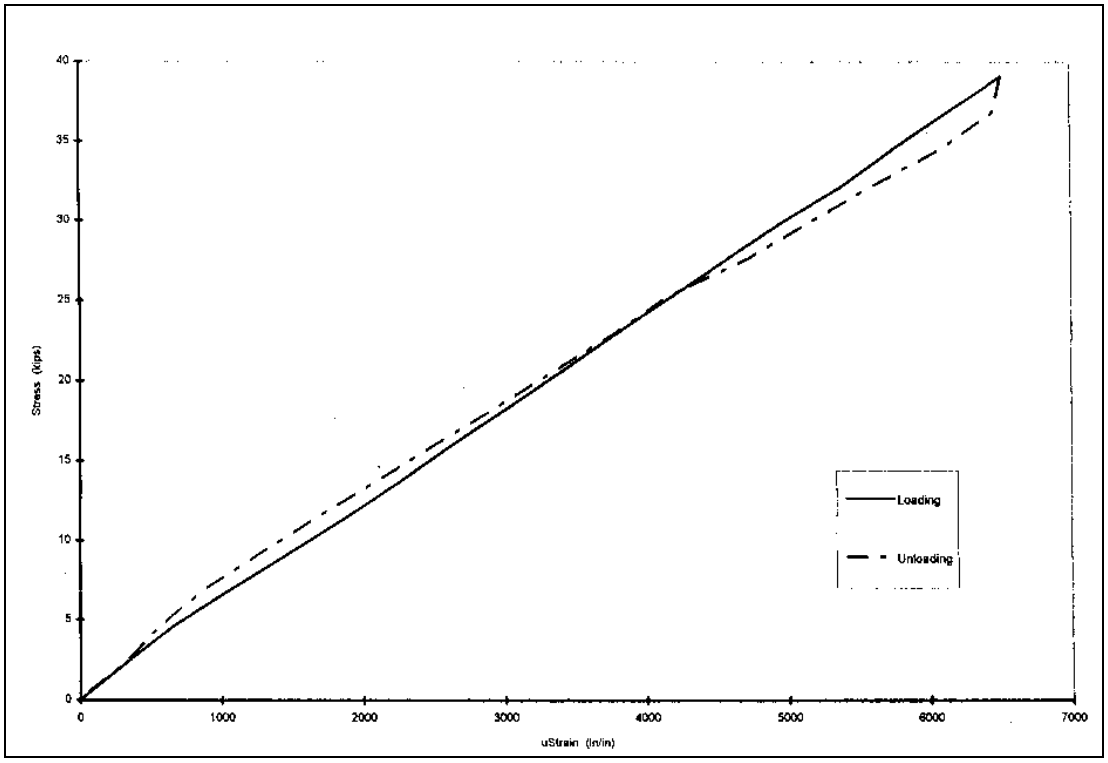

Figure 2.7. Typical stress-average strain plot for WF-FRP composite columns.

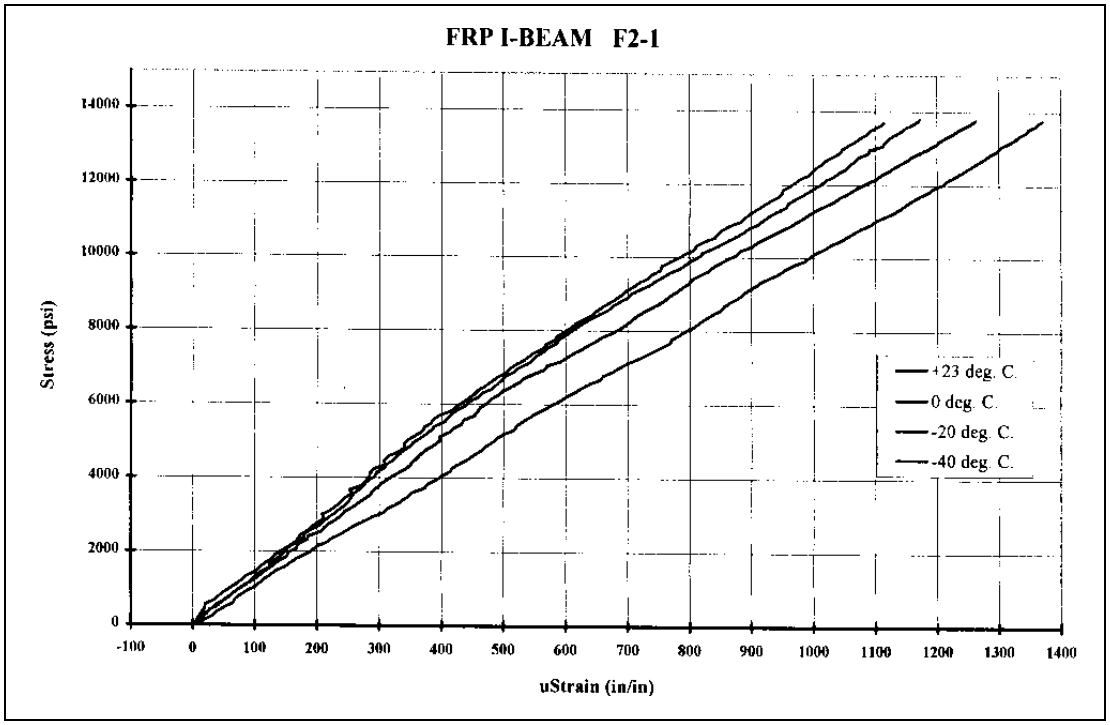

Figure 2.8. Typical stress-strain plots at various temperatures between 23 °C and -40 °C for WF-FRP composite columns.

Table 2.1. Fiber architecture for beam specimens.

Component Dimensions	Rovings	Fabrics and CSM	
	AC1 and A2	AC1	A2
Flange	r: 54 per ft	f1, f2, f6, f7: 18 oz 0/90 & ¾ oz CSM f3, f4, f5: 18 oz ±45 & ¾ oz CSM	f1, f2, f3, f4, f5, f6, f7: 18 oz ±45 & ¾ oz CSM
Web	r: 56.3 per ft	w1, w2, w7, w8: 18 oz 0/90 & ¾ oz CSM w3, w4, w5, w6: 18 oz ±45 & ¾ oz CSM	w1, w2, w3, w4 w5, w6, w7, w8: 18 oz ±45 & ¾ oz CSM

Table 2.2. Apparent modulus of elasticity as a function of fiber architecture for beam tests.

Bending test L = 19 ft	Fiber Architecture	E_{app} (10^6 psi)	% Improvement Over Existing
Strong axis (x-x)	AC1* A2*	3.95 3.75	40.9 34
Weak Axis (y-y)	AC1 A2	4.29 4.10	53.4 46.4
*Note: AC series bidirectional cross-ply plus angle-ply; A series bidirectional angle-ply only.			

Table 2.3. Summary of the results of local buckling tests on optimized columns.

"Off-the-Shelf" Samples			F1 Fiber Architecture Samples			F2 Fiber Architecture Samples		
Sample	Label	Load (kip)	Sample	Label	Load (kip)	Sample	Label	Load (kip)
1	CP1	155	1	F1A	209	1	F2A	261
2	CP2	159	2	F1B	207	2	F2B	255
			3	F1C	214	3	F2C	266
			4	F1D	216	4	F2D	250
			5	F1E	216	5	F2E	256
			6	F1F	217	6	F2G	251
			7	F1G	215	7	F2G	250
			8	F1H	223	8	F2H	260
	# Samples	2		# Samples	8		# Samples	8
	Ave.	157		Ave.	214.63		Ave.	256.13
	STD	2.83		STD	4.93		STD	5.84
	95% Conf	3.92		95% Conf	3.41		95% Conf	4.05
	% Incr.	--		% Incr.	37%		% Incr.	63%

Table 2.4. Summary of optimized column compressive tests.

Sample	Geokon (Single Cycle)	MTS, (3 load/unload cycles to 30% failure.)			
	+23 deg. C.	+23 deg. C.	+23 deg. C.	+23 deg. C.	+23 deg. C.
F1-2		X	X	X	X
F1-4		X	X	X	X
F1-16	80% Failure E = 7.73e6 psi	X	X	X	X
F2-1	80% Failure E = 6.01e6 psi	X	X	X	X
F2-2		X	X	X	X
F2-3		X	X	X	X
F2-6	100% Failure σult = 47,278 psi				

3 Shape, Fiber Architecture, and Fastening System Optimization of New Shapes

Theoretical Optimization

Analytical modeling techniques were used to optimize both shape and fiber architecture. Optimization criteria included improving load capacity and stiffness compared to current market products with the same cross-sectional area, or achieving a similar load capacity and stiffness with substantially smaller cross-sectional area to current market products. The analytical models led to two linear shapes and one planar shape. The linear shapes included one for beams and one for columns. The beam shape was called a "winged box" (WB) and the column was called a "unicolumn" (UC). The planar shape was optimized for bridge deck applications. The planar shape optimization led to a new shape called the hexagonal deck, or H-Deck (Figure 3.1). This new structural shape can be used as an individual beam element or assembled to create an orthotropic deck. Of the three theoretical optimized shapes, the H-Deck was the only shape to be produced and experimentally evaluated.

Manufacturing the New Optimized Shapes

Two different manufacturing processes have been used to produce the H-Deck during the laboratory prototype experiments. In both processes, an efficient fiber architecture was designed with several layers of multiaxial fabrics in a vinyl ester matrix.

VARTM

H-Deck prototypes were manufactured by Vacuum-Assisted Resin Transfer Molding (VARTM). Some aspects of this manufacturing process are patented as SCRIMP™ (Seeman Composites Resin Infusion Molding Process). This manufacturing process requires minimum tooling and can be used to fabricate large deck modules. Heavyweight multiaxial stitched fabrics (up to 64 oz/yd^2) with chopped strand mats manufactured by Brunswick Technologies Inc. (BTI) were used as reinforcements. Foam was used as tooling to mold the cells in the

VARTM prototypes. In this VARTM process, the fabrics are laid up dry by hand, then a vacuum is applied and resin is infused. The disadvantages of this fabrication process for the proposed FRP deck are that it is labor-intensive and that product uniformity is difficult to maintain, the latter resulting in higher dimensional tolerances. These disadvantages can be partially overcome by using more expensive tooling and more efficient production techniques such as fabric pre-forms. Fiber volume fraction ranging from 50 to 55 percent were attained. The test prototypes were fabricated by Hardcore-Dupont Composites, LLC (New Castle, DE). Four modules that were 10'x3.75'x8" and four that are 2'x3.75'x8" were received for test purposes. After the initial prototypes were produced, Hardcore-Dupont withdrew their support for the project and no additional H-Deck sections were produced by the VARTM process.

Pultrusion

H-Deck modules for laboratory testing and field demonstration were also fabricated by pultrusion. The main disadvantage of pultrusion is the initial high cost of tooling. As noted earlier in the discussion on fiber architecture for existing structural shapes, it was demonstrated that a pultruded wide-flange beam, with efficient bi-directional fiber architecture exhibited enhanced stiffness response, and ensured fiber continuity between flange and web elements. Based on this new fiber architecture concept and the pultrusion expertise that was developed, pultruded sections equivalent to the VARTM prototype were designed. Creative Pultrusions, Inc., fabricated two dies and pultruded double-trapezoid and hexagonal components. Figure 3.1 shows a diagram of H-Deck components and a photograph of how the components fit together. Deck components were pre-assembled at the factory under controlled conditions using a two-part polyurethane adhesive (PLIOGRIP® 6600) between the individual elements. The selection of the adhesive was based on tests discussed later in this chapter.

The efficient fiber architecture of the pultruded components incorporates rovings and triaxial stitched fabrics with binderless CSM that were custom-designed and fabricated by BTI. The triaxial stitched fabric weighs 40 oz/yd^2. The advantages of pultrusion are: (1) low labor cost, (2) low operating costs, (3) minimal material wastage, and (4) high production rate. Assuming a composite material density of 110 lb/ft^3, the pultruded H-Deck weighs $20lb/ft^2$.

New Optimized Shape Experimental Testing

Tests Series Design Criteria and Test Setup

A test program was developed for evaluating the applicability of both the VARTM and pultrusion H-Deck systems for bridge deck applications. The AASHTO LRFD* bridge design specification provided the basic criteria used in designing the tests series. Tests were conducted to determine longitudinal stiffness and the effect of repetitive simulated wheel loads on the long-term integrity of the decks. All H-Deck tests were conducted as simply supported beams with a maximum free span of 9 ft. The 9 ft length was selected as an upper bound for the deck span between stringers in the AASHTO HS20 design truck live load (See Appendix A). The span length was oriented in the direction of maximum stiffness (parallel to the cell direction as illustrated in Figure 3.2). Prior to the wheel load tests, transverse line loads, with a load width of 11.5 in., centered on the 9 ft span, were used to establish longitudinal stiffness for the VARTM deck system. The longitudinal stiffness of the pultrusion system was determined in a similar manner, but the individual components—the double-trapezoid and hexagon—were tested as opposed to the complete deck. The longitudinal stiffness was then computed assuming composite action between the pultrusion modules (Table B1, Appendix B). The longitudinal stiffness data were used for assessing compliance with AASHTO deck deflection criteria.

The setup for the fatigue tests (repetitive simulated wheel load) consisted of simply supporting the deck specimens on 3 in. diameter solid steel bars spaced 9 ft apart. The steel bars were confined by steel channels. The bars allowed the deck sections to rotate at the end supports without transferring moment or secondary horizontal forces between the end supports and the test specimen. Steel sheet stock 4 in. wide by 0.25 in. thick was placed between the deck and the steel bar to transfer the bar load to the deck modules. The simulated tire load was a rectangular 20 in. x 10 in. steel plate of 2 in. thickness. A 20 in. x 10 in. x 0.5 in. rubber pad was placed between the deck and the steel loading plate. The rubber pad was used to minimize abrasion between the 20 in. x 10 in. steel loading plate and the composite deck during the fatigue tests.

* AASHTO is the American Association of State Highway and Transportation Officials. LRFD is load and resistance factor.

AASHTO criteria were used for selecting the dimensions of the rectangular tire patch and the selected load and duration of the tests (Appendix A). Figure 3.2 illustrates the locations of the loading plate and reactions for the fatigue test series. The larger loading plate dimension was always perpendicular to traffic flow. The test setup for the VARTM and pultrusion decks were identical, with the exception that the VARTM deck sections were 45 in. wide and the pultrusion decks were 36 in. wide. To accommodate the different widths, two different fatigue load ranges were used: 5 to 50 kips for the VARTM deck and 2 to 35 kips for the pultrusion deck (see Appendix A). The limit for the fatigue tests was set at 2 million cycles in accordance with AASHTO criteria for highway bridges in rural areas. See Appendix A for details.

The fatigue tests were conducted with a 50 kip closed-loop hydraulic actuator mounted on a heavy structural steel frame (Figure 3.3). A sinusoidal loading function was used for the fatigue tests at a loading rate of three cycles per second.

The fatigue test specimens were not expected to fail during the 2 million cycles, thus the analysis focused on assessing the structural degradation associated with the cyclic loading. Two measures were used to assess degradation: (1) changes in stiffness and (2) failure loads. To assess changes in stiffness of the decks, static load deflection measurements were made on the H-Deck specimens before the fatigue tests, and after every 0.5 million cycles up to the 2.0 million fatigue cycles. The second degradation criteria was measured by loading to failure the test specimens that had previously been fatigued for 2 million cycles and comparing those strengths with similar tests performed on specimens with no previous load history. The static load-deflection measurements used the same loading equipment (50 kip closed loop hydraulic actuator) that was used for the fatigue tests. The peak load for the static load-deflection tests was the peak fatigue load — 50 kips for the VARTM and 35 kips for the pultrusion specimen. The loading rate for the static load-deflection tests was 5 kips per minute. A Southwark Emery 3 million lb testing machine at the University of Illinois, Urbana-Champaign was used in the failure tests (Figure 3.4). The basic loading setup for the failure tests was the same as used in the fatigue and load deflection measurements (see Figure 3.2). The loading rate for the failure tests on the two VARTM deck specimens was between 10 and 25 kips per minute: for the pultrusion deck specimens, the loading rate ranged from 2 to 5 kips per minute.

A Hewlett Packard 3052A data acquisition system was used for collecting the load, deflection, and strain data during the static load-deflection measurements. Before the fatigue tests began each deck was outfitted with 14 strain gages. In

addition, 15 LVDTs were attached to an independent steel tubing frame suspended above the deck. All LVDTs were positioned perpendicular to the plane of the deck before each static loading test cycle. The locations where the LVDTs contacted the decks were marked before the initial static load deflection tests and adjusted as needed for the subsequent load deflection tests on each deck. The LVDTs measured the vertical displacement of the deck top during the static load tests. Yoyo gages were placed under the decks to measure bottom side deflection during the static tests. Figures 3.5 and 3.6 present the relative location of the various deflection and strain gages for the VARTM and pultruded decks, respectively. During fatigue cycling the LVDTs were capped and the yoyo gages were disconnected, thus not subjecting either gage system to cyclic loading rigor and degradation. However, the strain gages were subjected to cyclic loading as they were adhered to the surfaces of the H-Deck before testing began.

Analysis and Discussion of Tests Results

The visual analysis of the VARTM and pultrusion fatigue test specimens indicated that no observable degradation occurred to either deck system during the 2 million fatigue cycles. Changes in stiffness were assessed by comparing the relative deflections (midspan and quarter-span vertical displacement minus the average of the vertical displacements over the end reactions) obtained at the peak static loads during the static load deflection tests. Figure 3.7 presents the relative vertical deflections in the longitudinal direction for the five static tests (before fatigue and after every 0.5 million fatigue cycles) on the VARTM deck. Figure 3.8 presents the relative vertical deflections for the five static tests in the transverse direction for the VARTM deck. Figures 3.9 and 3.10, respectively, are the longitudinal and transverse relative deflections for the five static tests for the pultrusion deck. A visual analysis of Figures 3.7 through 3.10 is inconclusive in determining if there was a degradation of stiffness during the 2 million fatigue cycles, but the figures do indicate that any stiffness degradation which might have occured was very minor. A least-squares linear regression analysis and an analysis of variance (ANOVA) test was conducted on the static deflection data relative to the number of fatigue cycles. The ANOVA analysis is presented in Table 3.1. The p-test within the ANOVA is used to determine the statistical significance of the relationship between the two variables—number of fatigue cycles versus relative deflections at peak static load. P values near 0 indicate good correlation and P values near 1 indicate no correlation. A review of Tables 3.1 and 3.2 indicates that for both the VARTM and pultruded decks, the fatigue level did not significantly correlate to changes in maximum deflections. Thus it is concluded for the data analyzed there was no statistically significant relationship between the relative deflections at peak static load and the number of fatigue cycles. Several factors may have contributed to the minor

nonuniformity in the peak static deflections. These factors include drift in the calibration of the LVDTs, variations in span length associated with slippage of the steel bar end supports, and changes in the ambient temperature during the static load-deflection tests.

The second assessment of fatigue degradation was the load test to failure for fatigued versus non-fatigued (no prior load history) specimens. Figures 3.11 and 3.12 present the load versus mid-span relative-deflection curve for the VARTM decks and pultrusion decks, respectively. The failure loads for the VARTM decks were 267.5 kips and 269 kips, respectively, for the fatigued and non-fatigued specimens. The failure loads for the pultrusion decks were 124.5 kips and 126.7 kips, respectively, for the fatigued and non-fatigued specimens. In both the VARTM and pultrusion deck systems the fatigued specimens failed at a lower loads than did the specimens with no prior load history, but the differences between the fatigued and non-fatigued specimens were so small that it is assumed to be negligible. The observed stiffness values of the fatigued and non-fatigued specimens also were nearly identical for both the VARTM and pultrusion deck systems. Thus, as with the stiffness analysis conducted on the static load deflection data, the number of fatigue cycles did not appear to significantly affect either the ultimate deck strength or stiffness.

Both the strength and the failure modes for the VARTM and pultrusion decks were significantly different. The failure loads of the VARTM decks were nearly double those for the pultruded decks even though the width of the VARTM deck was only 25 percent greater. The failure mechanisms of both VARTM decks appeared to be local compressive buckling of the upper flange and compressive buckling or shearing of the web (Figures 3.13 and 3.14). The failures occurred in two distinct time phases. The initial phase occurred catastrophically and consisted of local compressive buckling and/or shearing just beyond the load plate, along its 10 in. width. The second phase occurred after the deck had lost approximately 20 percent of its original ultimate strength and continued to carry load. This second phase was the expansion of the local compressive buckling of the upper flange near the loading plate to compressive buckling across the remaining width of the upper flange of the deck.

For the pultrusion decks there was a combination of two failure mechanisms: (1) longitudinal shear failures along the entire length of the H-Deck, between adjacent double trapezoid elements and through the hexagon keys, and (2) localized compressive and shear buckling under the loading plate (Figures 3.15, 3.16, and 3.17). The localized buckling under the loading plate occurred in the walls of the hexagon key and the adjacent web of the double trapezoid elements. For the most part the longitudinal shear failures were not adhesive failure but

interlaminar tearing between the layers of glass fiber lay-ups. The longitudinal shear failures degraded the level of composite action between the three double-trapezoid elements.

As previously noted, the failure loads for the VARTM decks were considerably higher than those achieved for the pultrusion decks. Even when the differences in the width of the two decks are factored in, the failure strengths are still significantly different. The pultrusion decks have lower strengths. The simple comparison based on deck width alone does not consider that in the VARTM tests the loading plate was spread over two adjacent double-trapezoid elements while in the pultrusion deck specimens, the loading plate was mounted over the middle double trapezoid element only. The continuous glass fabric on the decks of the VARTM specimens assured composite deck action and minimize the effect of the loading plate location relative to the locations of the hexagonal sections within a given deck. The pultrusion specimens, however, as they approach failure, lose their composite action; therefore, the specific location of the loading plate would probably influence the resulting strength measurement. In other words, the difference in the results of the two H-Deck system tests is that the pultrusion decks have joints every 12 in. (a trapezoid section) whereas the VARTM decks have joints only at the ends of the specific deck modules and behave as elements of 36 in., 48 in., 60 in., or some other width. Thus it appears that the tests on the pultrusion decks served as worst-case tests relative to the joint location while tests on the VARTM deck did not constitute a joint test at all.

The strengths of both deck systems, as subjected to the plate (simulated tire) load, significantly exceeded the live load for AASHTO HS20 (16 kips) and HS25 (20 kips) truck tire loads. Even for the HS25 live load the pultruded deck had a strength higher than six times the specified tire load, and it meets an $l/500$ deflection criterion for a 9 ft span. Additionally, fatigue degradation did not appear to occur in either deck system for the 2 million cycles at the applied loads.

Test and Evaluation of Fastening Systems for FRP H-Deck and WF Beams

Introduction

Connections play an important role in determining the capacity of a structure. When joining FRP composite structural profiles, the designer needs to account for the mechanical properties of connector materials as well as the

characteristics of the joining system. Bolted joints, adhesive joints, and combined bolted and adhesive joints can be used in FRP structures. The objective of this phase of the work was to develop design recommendations based on experimental evaluations for mechanical (steel bolts and anchors) and adhesive connections for FRP pultruded structural systems. The work presented in this section includes an evaluation of the effectiveness of steel bolts and steel sleeve anchors in double lap joints, adhesives in double lap joints, and adhesives in single lap joints. The details of the double lap joint test with bolts, anchors, and adhesives is documented (Sotiropoulos, GangaRao, and Lopez-Anido 1996). The material that follows summarizes the double lap tests, and provides details of the single lap tests.

Double Lap Joint Tests on Bolts, Sleeve Anchors, and Adhesives

Structural efficiency of the double lap joints was the criterion used for the double lap evaluation. Structural efficiency is defined as: $\Phi = \frac{P_u}{twF_{tu}}$

where P_u = ultimate load of joint

t = coupon thickness

w = coupon width

F_{tu} = unnotched tensile strength of the material.

For the bolted and sleeve anchors, structural efficiency was correlated with specimen width to bolt diameter $\left(tw/d\right)$ and end distance to bolt diameter ratio $\left(e/d\right)$. In the adhesive connections, structural efficiency was correlated with the adhesive length to inner adhered thickness.

Material test specimens were cut from pultruded multicellular panels and WF-FRP sections manufactured by Creative Pultrusions, Inc. The fiber volume fraction for the coupons varied from a high of 0.32 for the flange of the WF-FRP section to 0.25 for the web of the WF-FRP section. The fiber volume of the web and flange of the multicellular panel was 0.31. Fiber orientation was another variable evaluated for the WF-FRP sections. Traditional pultruded sections containing unidirectional rovings and CSM were compared with sections modified with bidirectional fabric lay-up. The difference between the modified sections and one of the standard sections is that two standard CSM layers were replaced by 0/90 and ± 45 stitched fabrics.

Joint coupons were cut in directions parallel and perpendicular to the major and minor fiber directions. Holes of 17/32 in. diameter were drilled at the center line of each specimen, at distances from the edge of 1 in. to 3 in., in half-inch increments for a half-inch diameter connector. The double lap test configuration is illustrated in Figure 3.18. The tests were configured to evaluate FRP composites connected to steel, thus two configurations were tested: a steel inner plate with composite outer plates and the reverse.

The adhesive joints used a two-part epoxy adhesive with a 2 hour pot life at 25°C. The surfaces were cleaned, sanded, and cleaned again with methyl alcohol before the application of the epoxy. The adhesives were applied in a 3 and 5 mil thickness. Figure 3.19 illustrates the adhesive test specimen. The test was configured to evaluate composites bonded to composites, so both the inner and outer plates were FRP composites.

All tests were conducted according to ASTM D953-87 (ASTM 1987). The joint efficiency of the bolted connections is evaluated from Figures 3.20 through 3.24 as a function of the edge-distance-to-connector-diameter ratio $\left(e/d\right)$ for various design parameters. Except where noted, the double-lap joints have two outer steel plates and one inner FRP plate with the main fiber direction parallel to the force direction. Figure 3.25 reveals joint efficiency for the adhesive tests. All adhesive joint specimens exhibited interlaminar mode of failure within the adherends. The interlaminar shear failure developed simultaneously, close to both bonded planes. In most cases the interlaminar failure developed in the outer plates of the joints between the outer CSM layer and the adjacent roving (unidirectional strands) layer of the WF section coupon. This mode of failure is attributed to shear failure of the binding polyester resin.

In the analysis, the optimal bolted joint is defined as the $\left(e/d\right)$ ratio beyond which no major increase in joint efficiency is observed. The optimal adhesive joint is likewise defined as the ratio of adhesive length to thickness of inner adherend beyond which no major increase in joint efficiency is observed. The optimum $\left(e/d\right)$ for the bolted joints was 4. At that $\left(e/d\right)$ with d/w = 0.249, a joint efficiency close to 40 percent was obtained when loaded along the main fiber direction, and almost 50 percent efficiency was achieved when loaded perpendicular to the main fiber direction. For the adhesive joint, the maximum joint efficiency of approximately 80 percent was obtained with a minimum adhesive-length to inner-adherend thickness ratio of 20.

Single Lap Joint Tests on Adhesives

The single lap joint tests were conducted to select an adhesive for bonding the double-trapezoidal and hexagonal pultruded sections. Performance criteria for adhesive selection included good elongation, high peel and energy-absorbing properties, fatigue resistance, environmental resistance (humidity, salt spray, temperatures of -20°F to 140°F), working time of at least 30 minutes, minimum surface preparation, acceptance of variable bond line thickness (30-120 mils), good gap-filling capabilities (to compensate fabrication tolerances), and ease of application for field conditions.

The specific dimensions of the coupons and the test specimen setup are illustrated in Figure 3.26. The tests evaluated three glue line thicknesses per ASTM D3165-95 and two moisture temperature conditions per ASTM D1151-90, at three repetitions for each test setup. Tests were conducted on two commercially available adhesives. PLIOGRIP® 6600, a two-part polyurethane from Ashland Chemical Co., and SIKADUR 30**,** a two-component high-modulus epoxy paste from Sika Corp. were used, Figures 3.27 and 3.28 show the shear strength to glue line thickness relationship for the SIKADUR 30 and PLIOGRIP® 6600 tests. The resulting shear strength of the PLIOGRIP® 6600 polyurethane adhesive was approximately double that of the SIKADUR 30 epoxy adhesive. Consequently, the PLIOGRIP® 6600 was the adhesive system used for bonding the double-trapezoidal and hexagonal pultruded sections both at the fabrication site and in the field. This adhesive was also used with the blind fasteners (BOM™ bolts, Huck International, Inc.) for attaching the H-Deck to the steel or composite stringers at the field demonstration sites, which are discussed in Chapter 4.

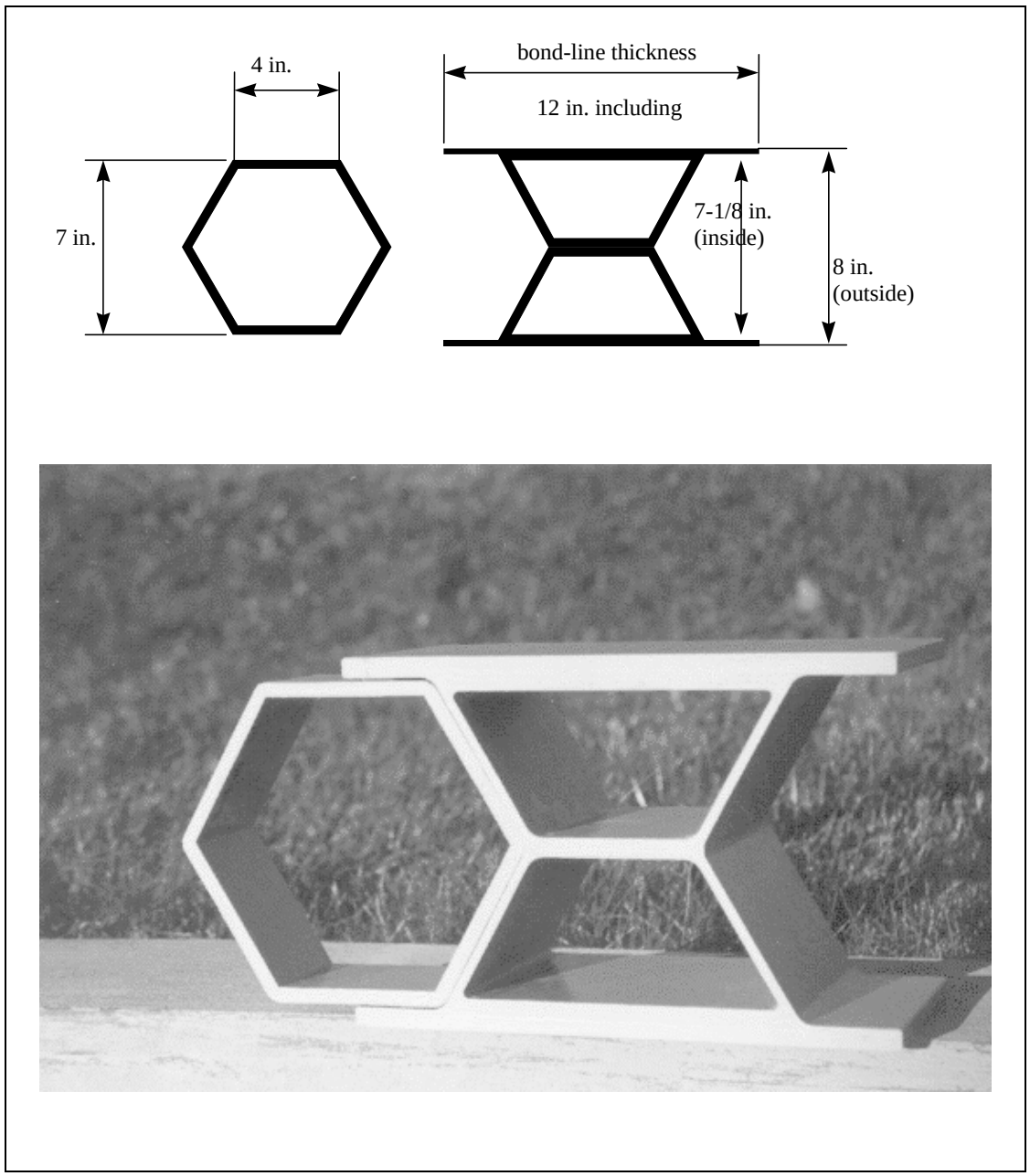

Figure 3.1. Diagram and picture of H-Deck components.

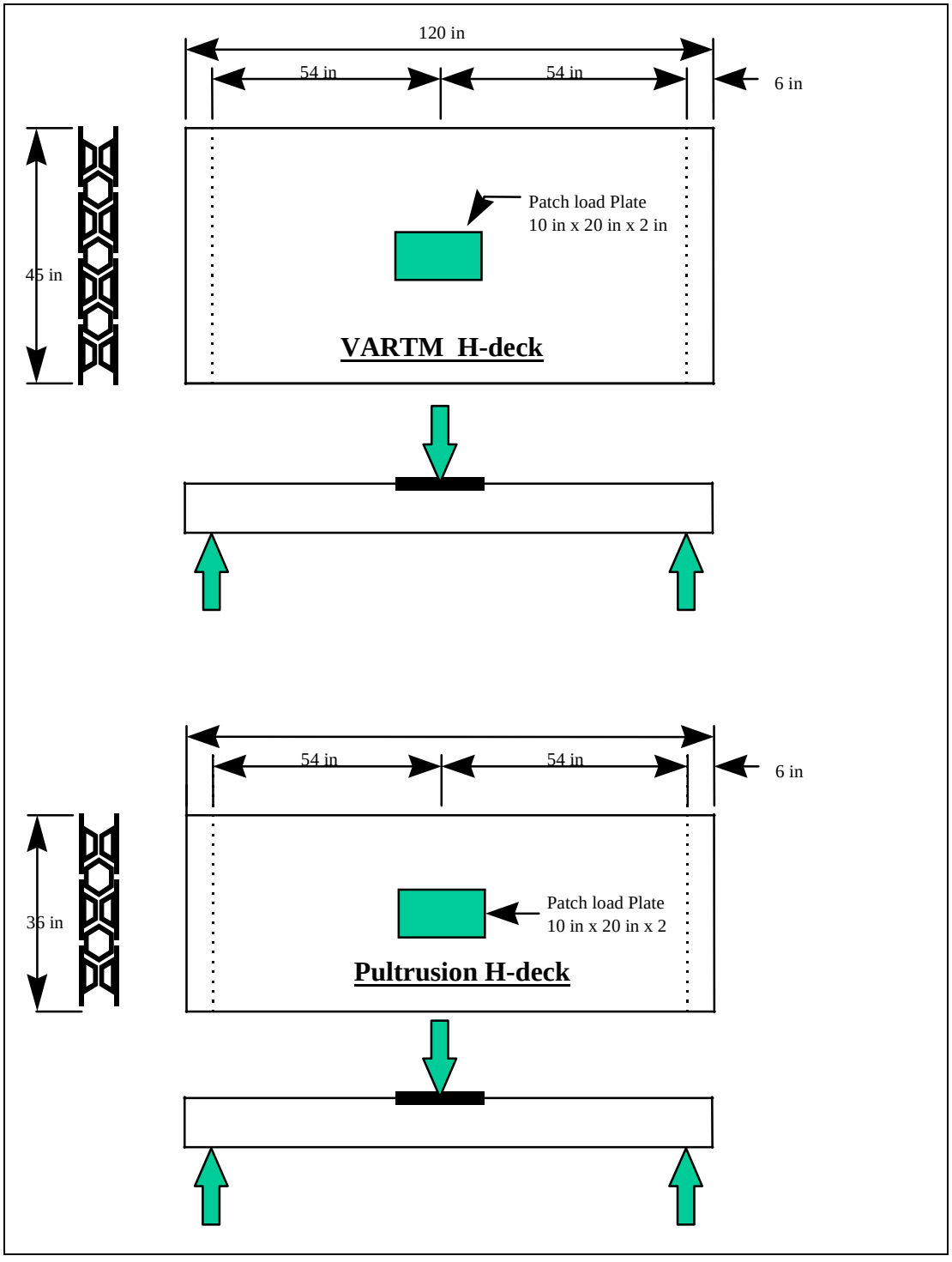

Figure 3.2. Fatigue test setup for VARTM H-Deck and pultrusion H-Deck.

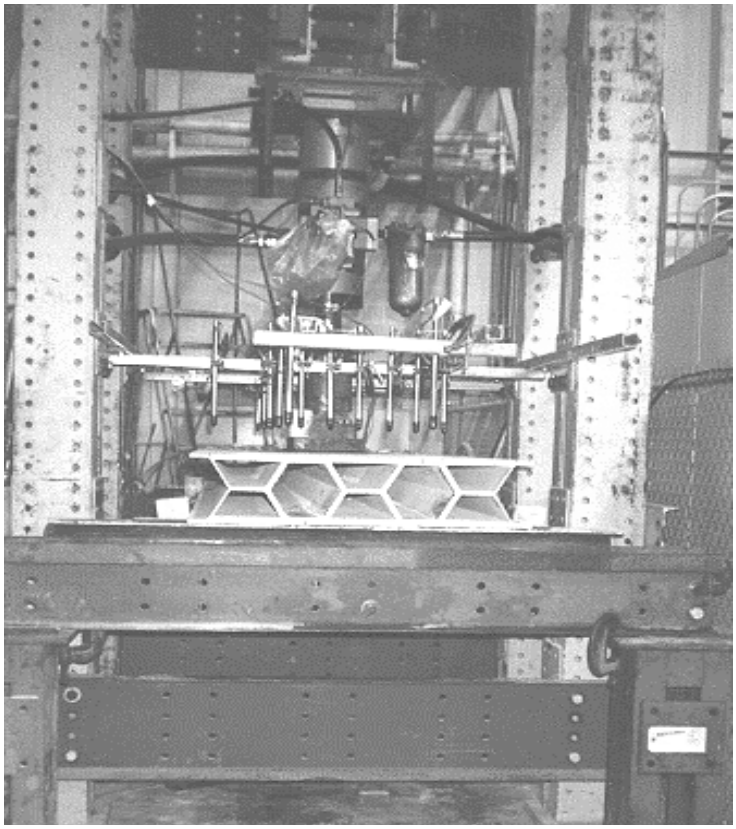

Figure 3.3. Fatigue test setup for H-Deck panels (pultruded section pictured).

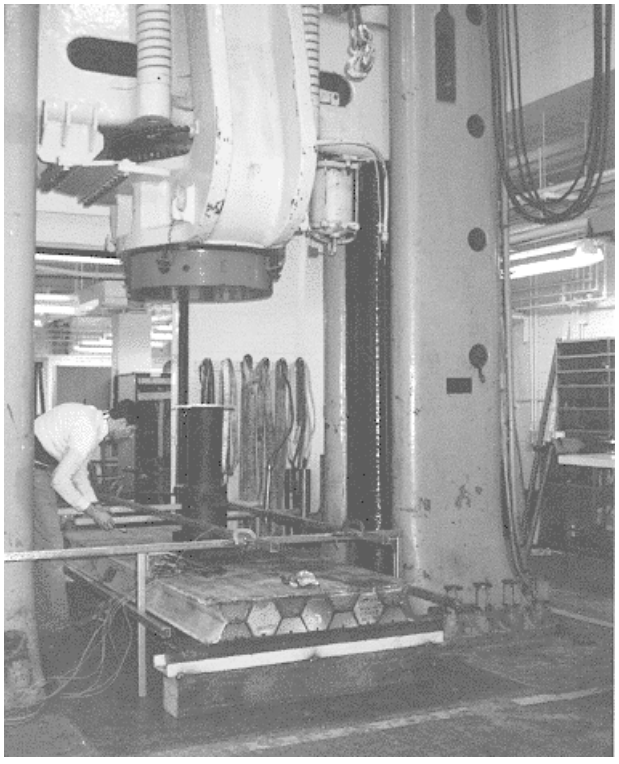

Figure 3.4. Failure test setup for H-Deck panels (VARTM section pictured).

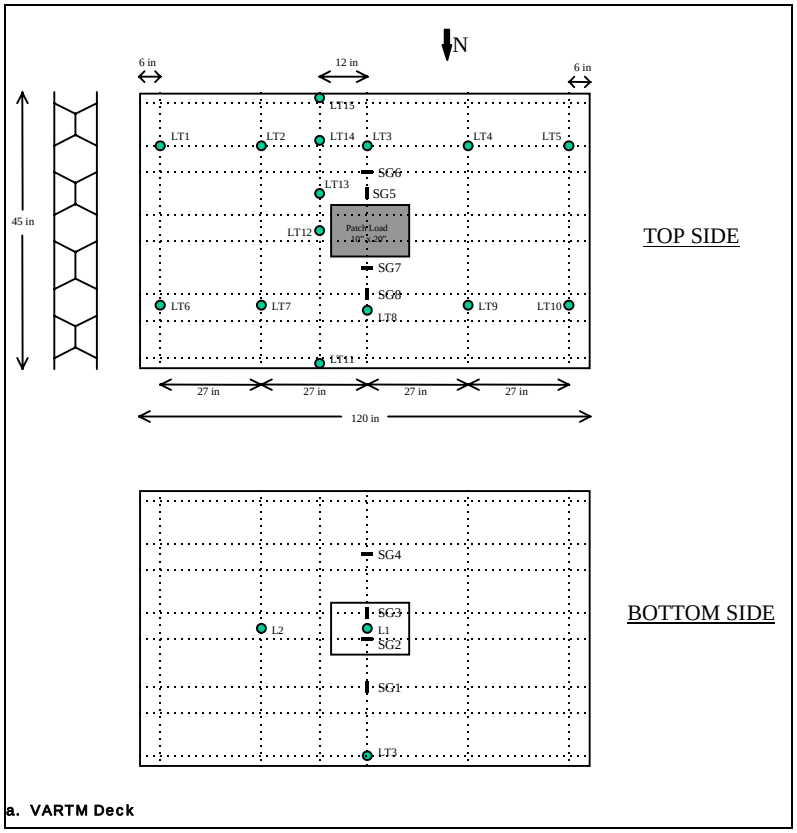

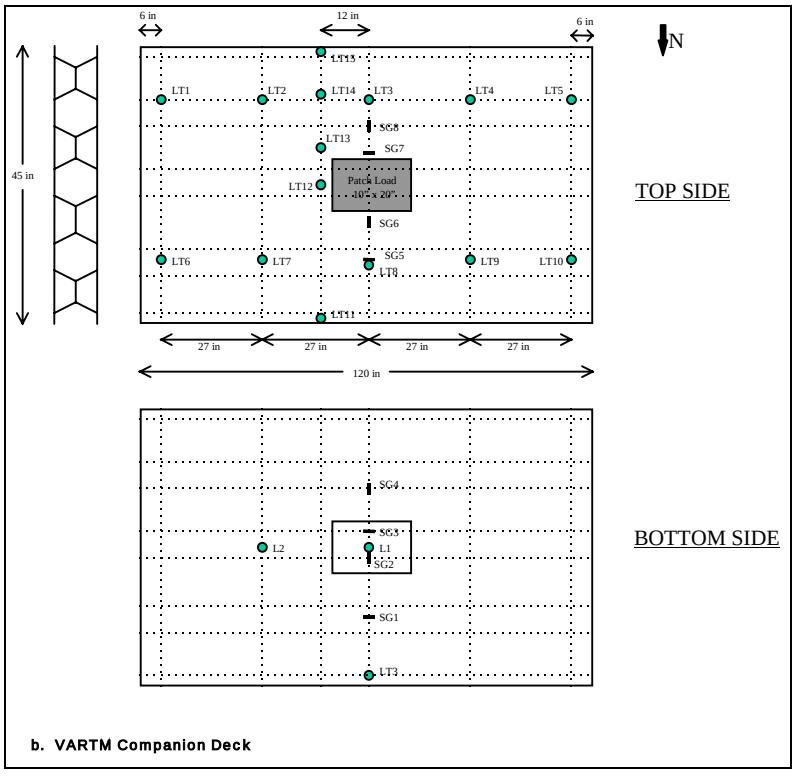

Figure 3.5. Location of LVDTs, yoyo gages, and strain gages for (a) VARTM and (b) VARTM companion decks.

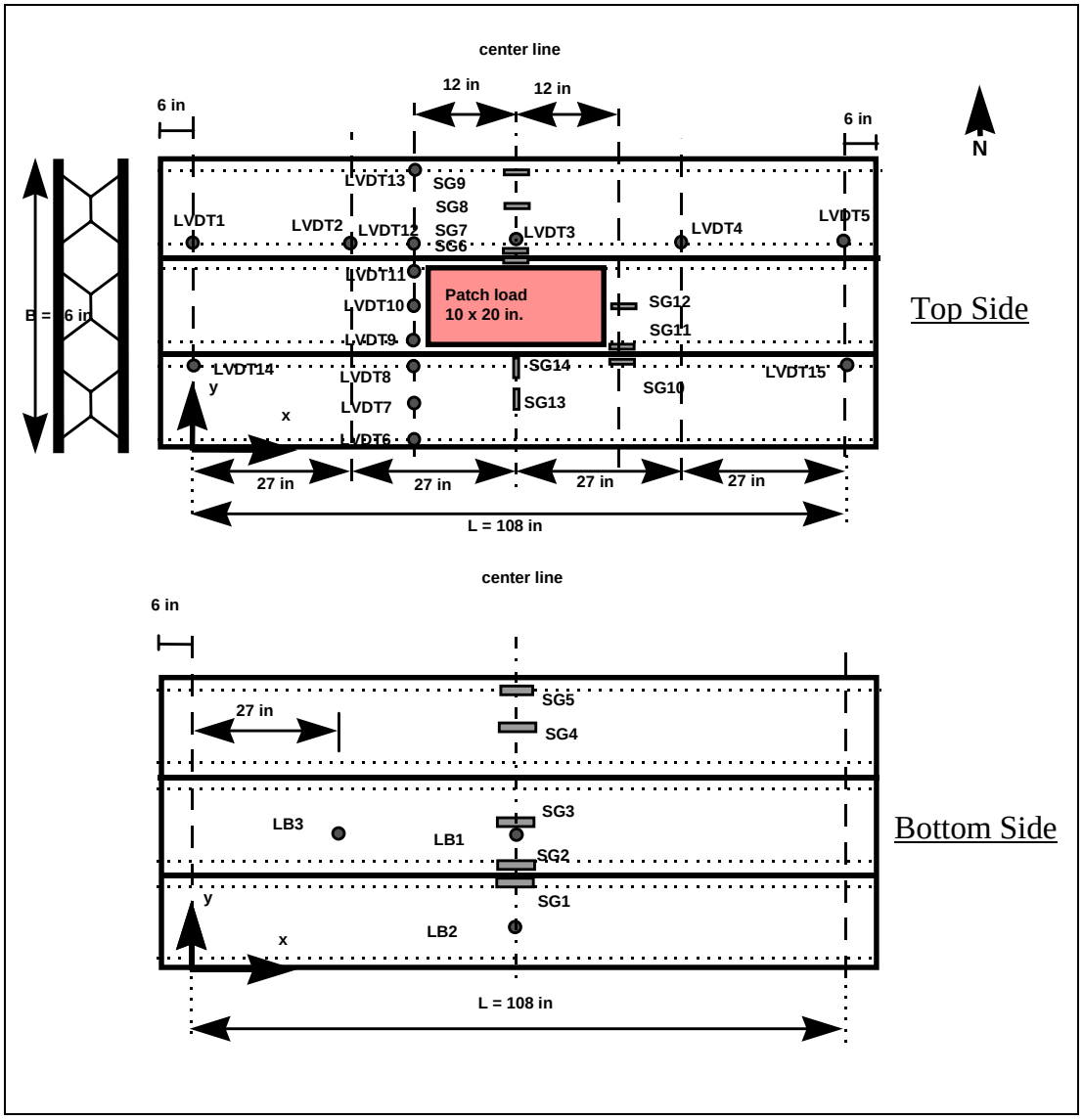

Figure 3.6. Location of LVDTs, yoyo gages, and strain gages for pultrusion H-Deck.

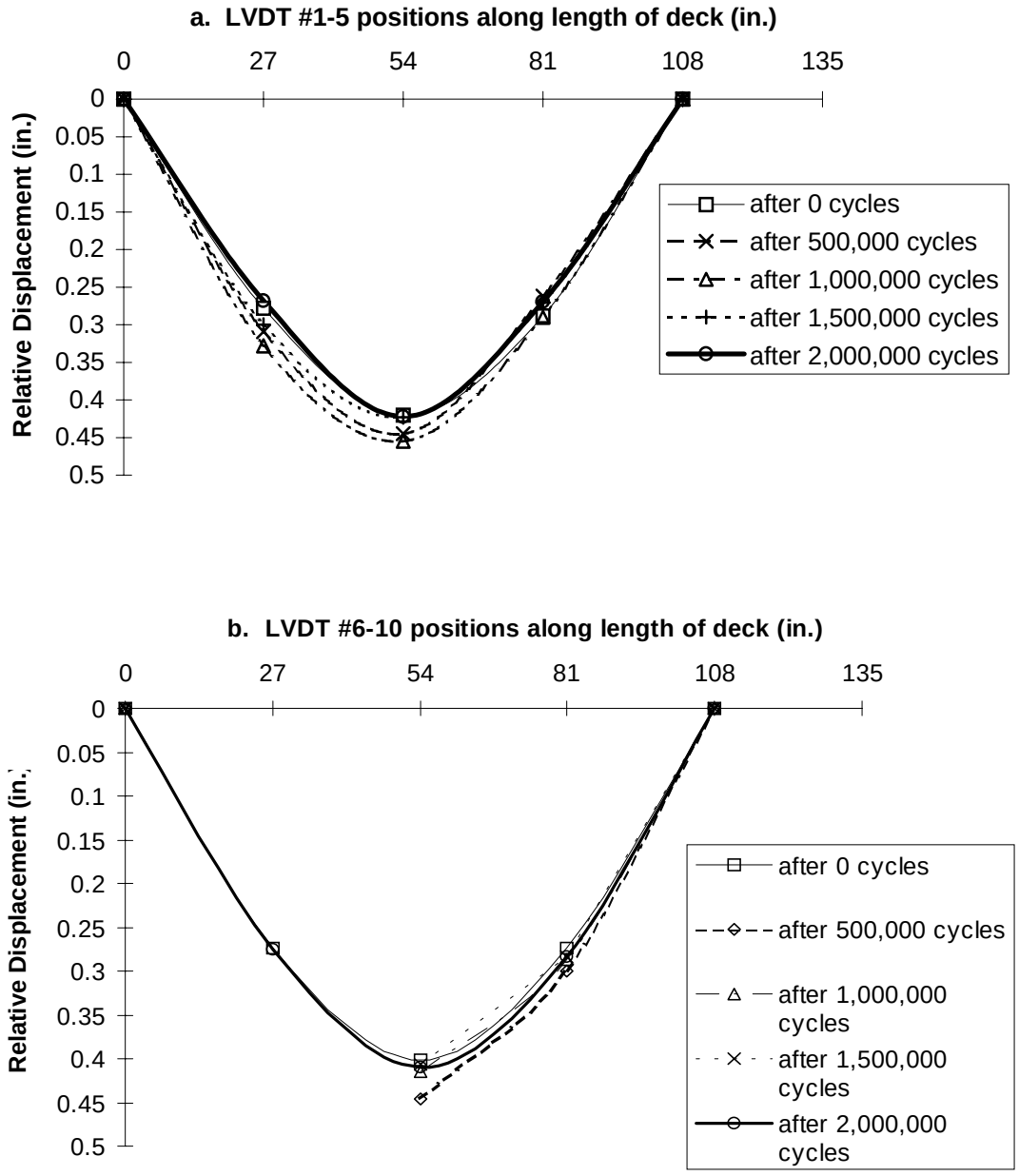

Figure 3.7. Plots of relative peak deflections for VARTM H-deck, static load-deflection tests for LVDTs (a) 1-5 and (b) 6-10.

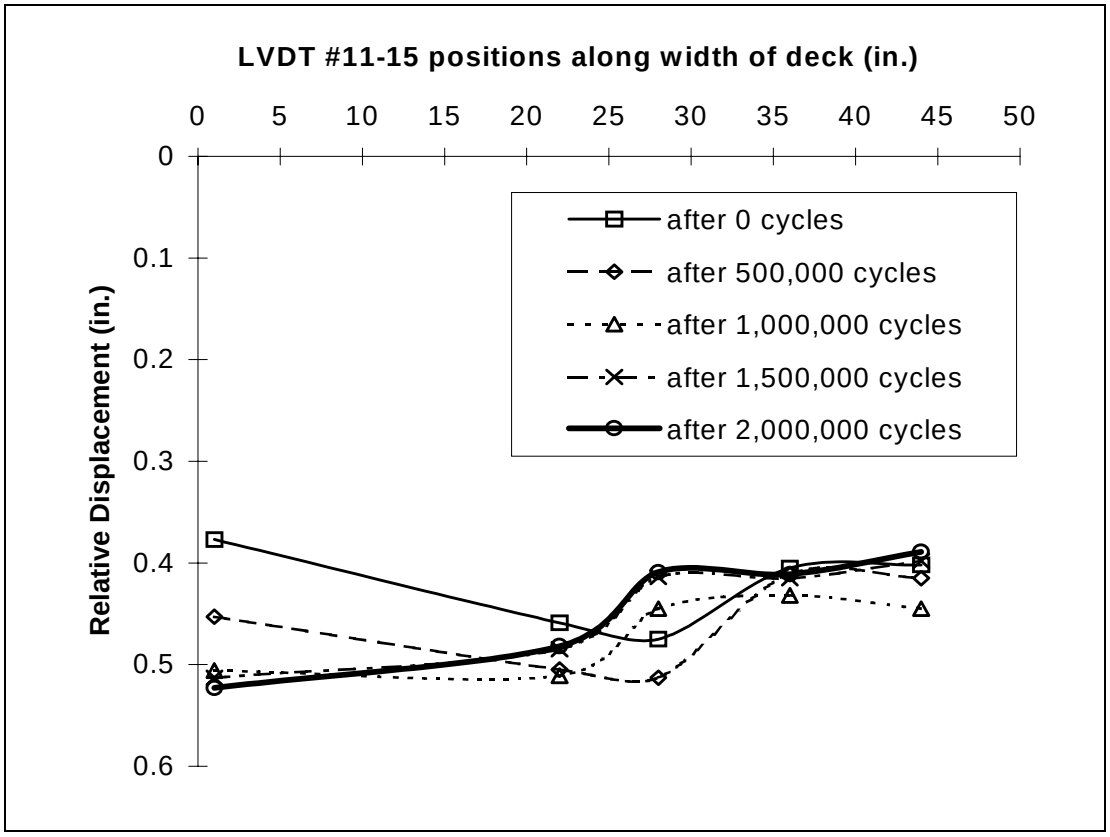

Figure 3.8. Plots of relative peak deflections for VARTM H-deck, static load-deflection tests for LVDTs 11-15.

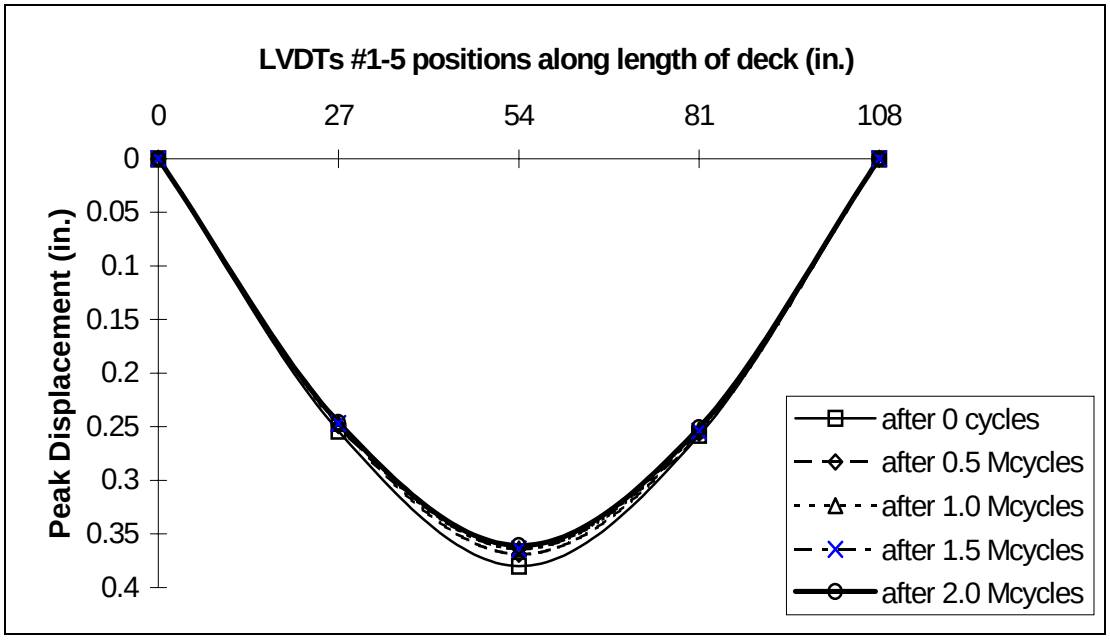

Figure 3.9. Relative peak deflections for pultrusion H-deck, static load-deflection tests for LVDTs 1-5.

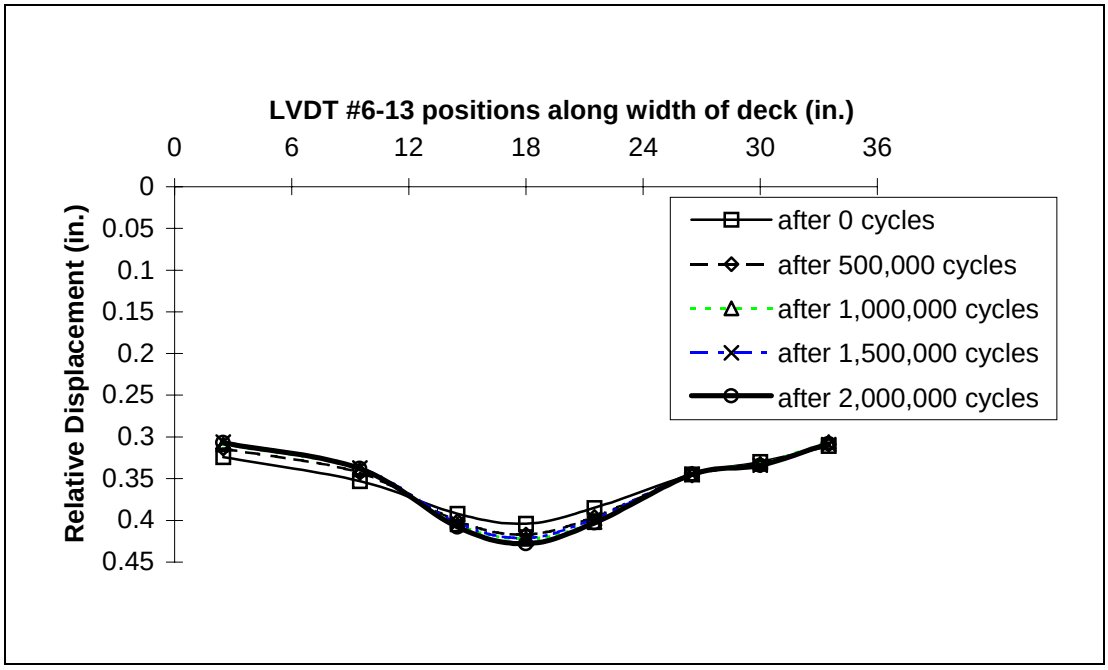

Figure 3.10. Relative peak deflections for pultrusion H-deck, static load deflection tests for LVDTs 6-13.

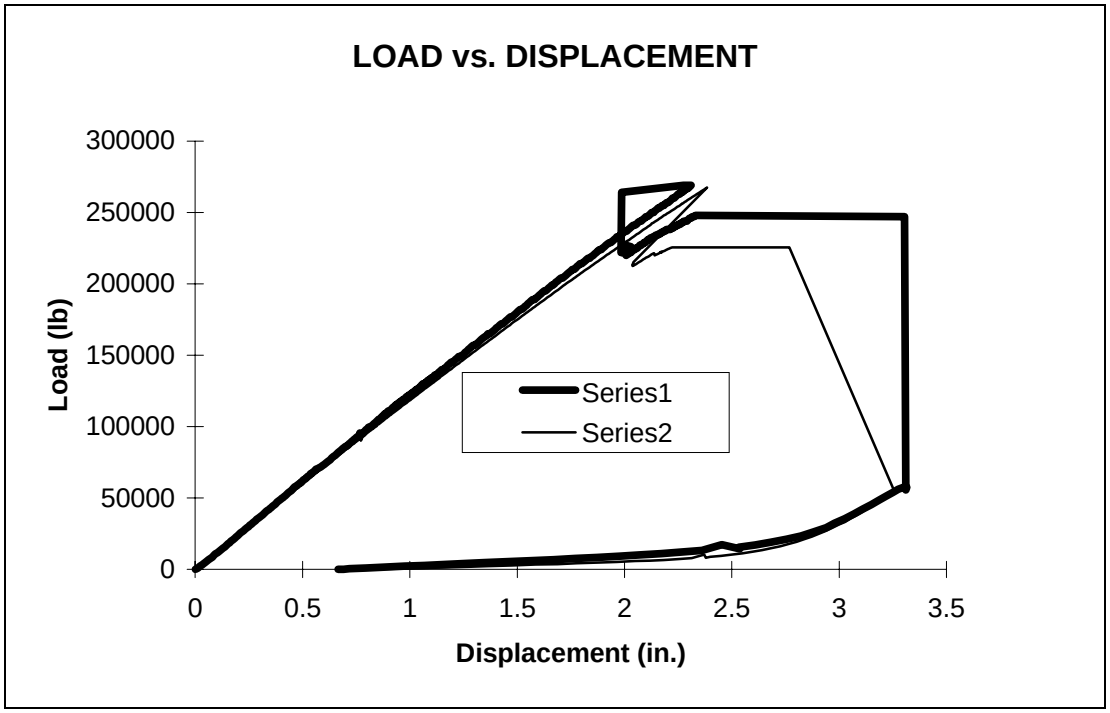

Figure 3.11. Failure tests of VARTM deck, load-displacement data for fatigued (Series 1) and non-fatigued (Series 2) specimens.

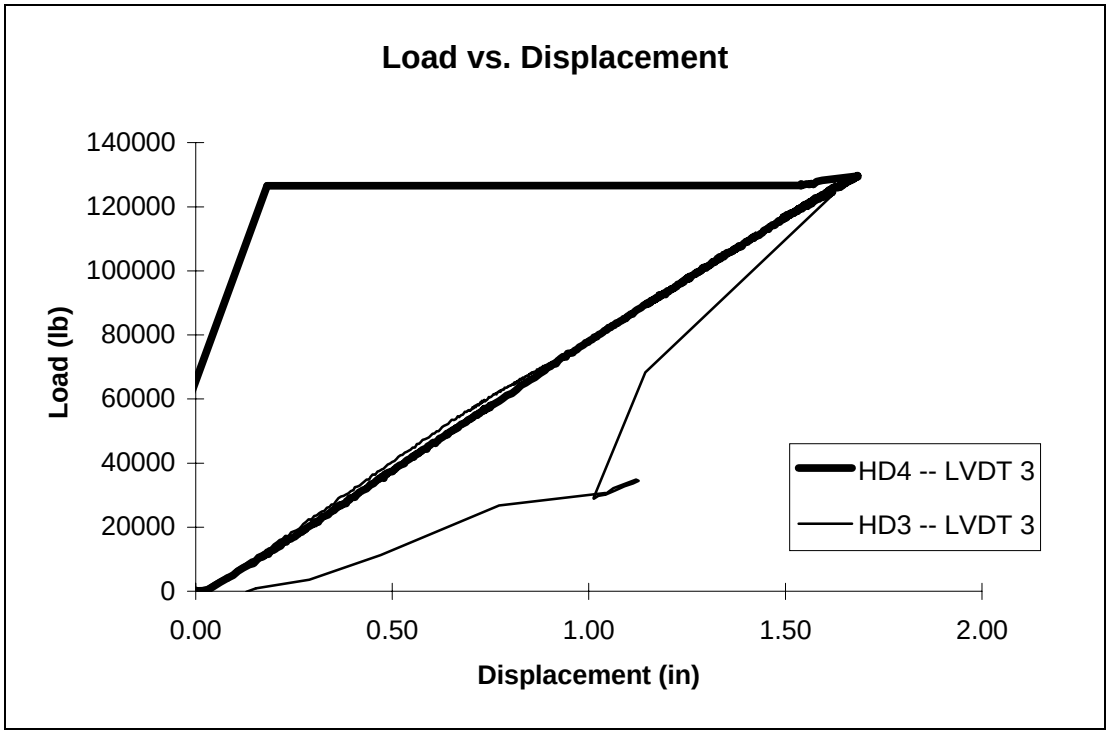

Figure 3.12. Failure test of pultrusion deck, load-displacement data for fatigued and non-fatigued specimens.

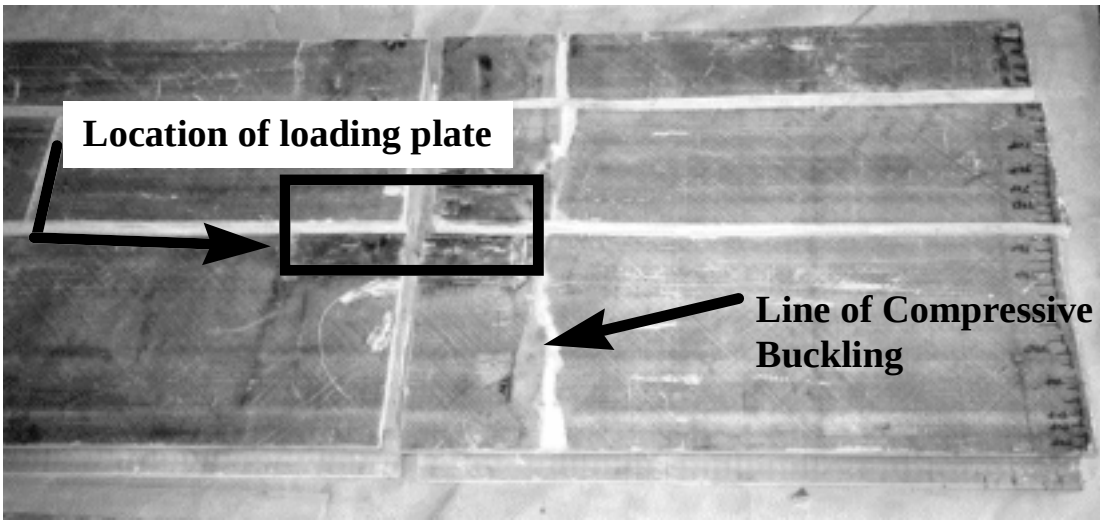

Figure 3.13. Section of VARTM H-deck after failure, showing line of compressive buckling just off the edge of loading plate.

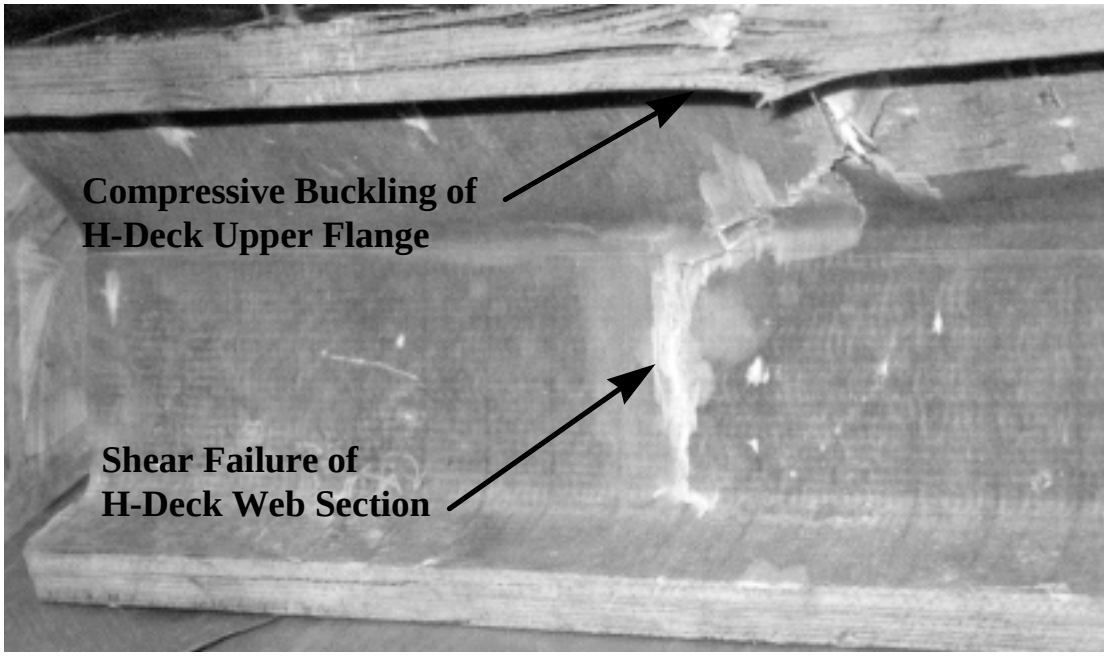

Figure 3.14. Close-up of VARTM H-Deck after failure showing compressive buckling of upper flange and shear or failure of web section.

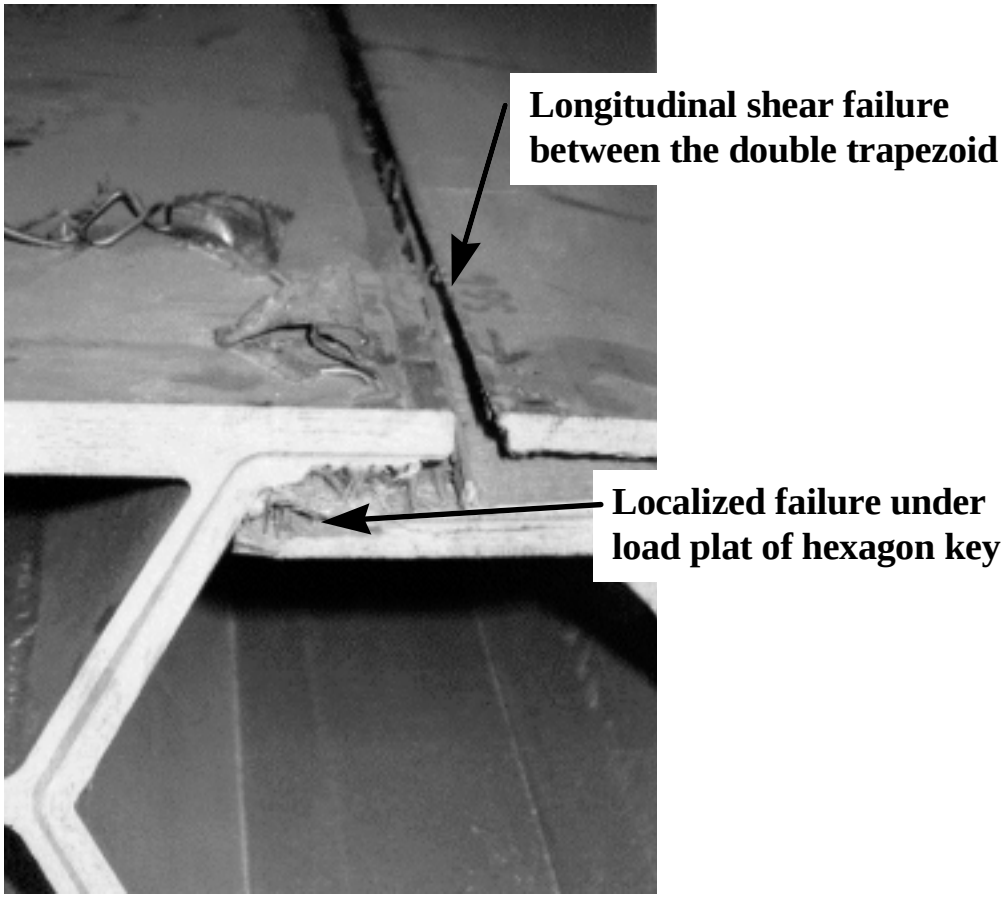

Figure 3.15. Close-up of pultrusion H-deck after failure showing shear key failure.

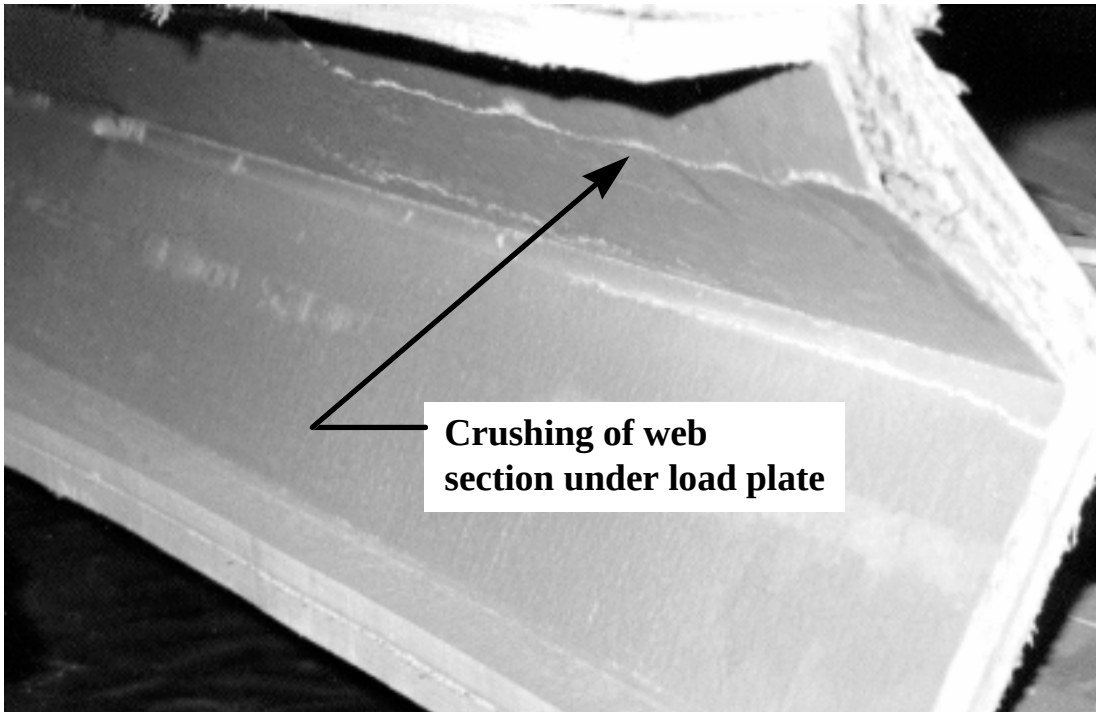

Figure 3.16. Close-up of pultrusion H-deck after failure showing crushing of web section under load plate.

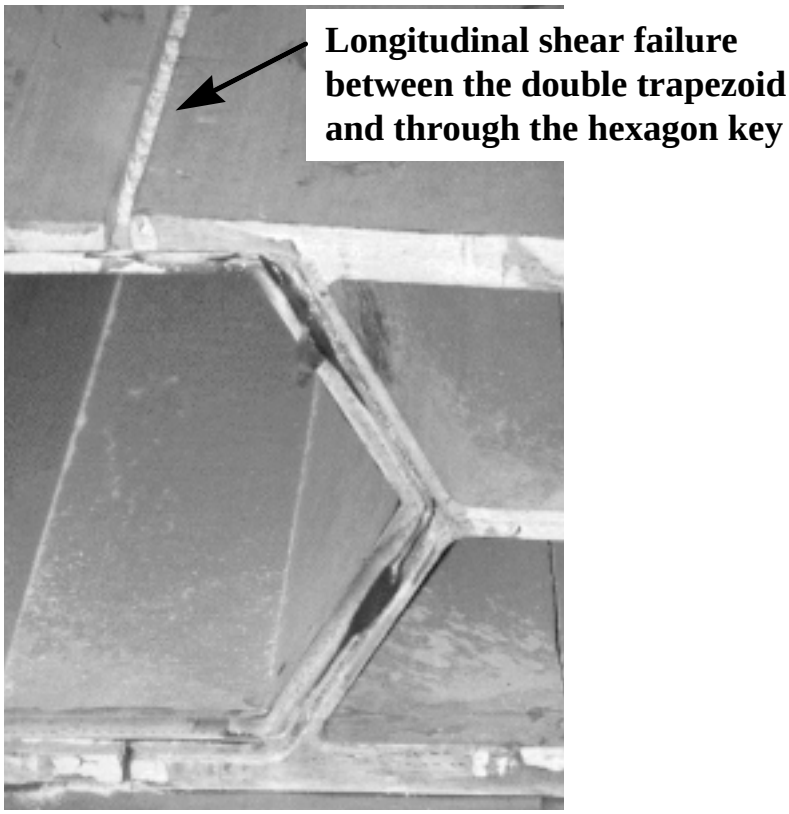

Figure 3.17. End view of pultrusion H-deck after failure showing portion of longitudinal shear failure at one end.

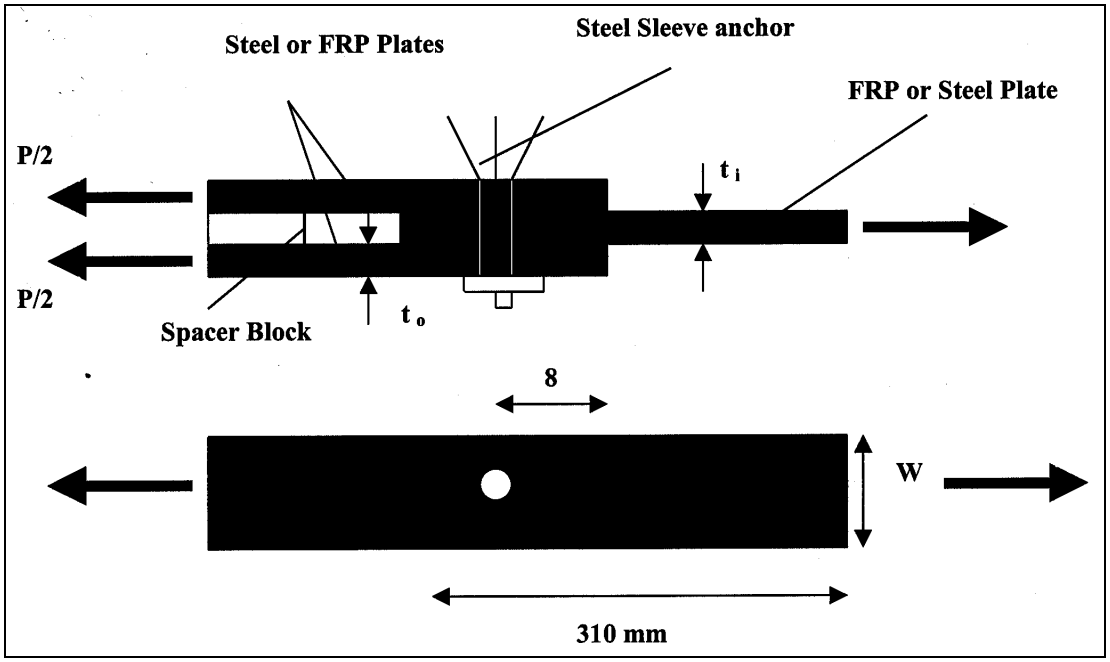

Figure 3.18. Setup of double-lap bolted joint with steel sleeve anchor connection.

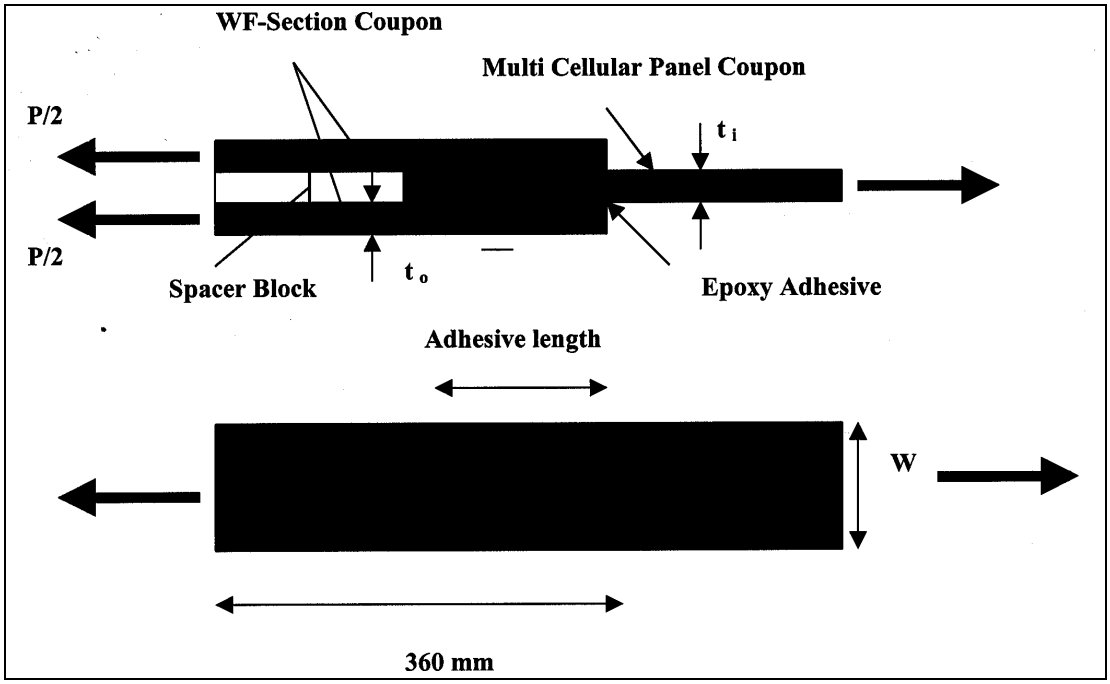

Figure 3.19. Setup of double-lap adhesive joint.

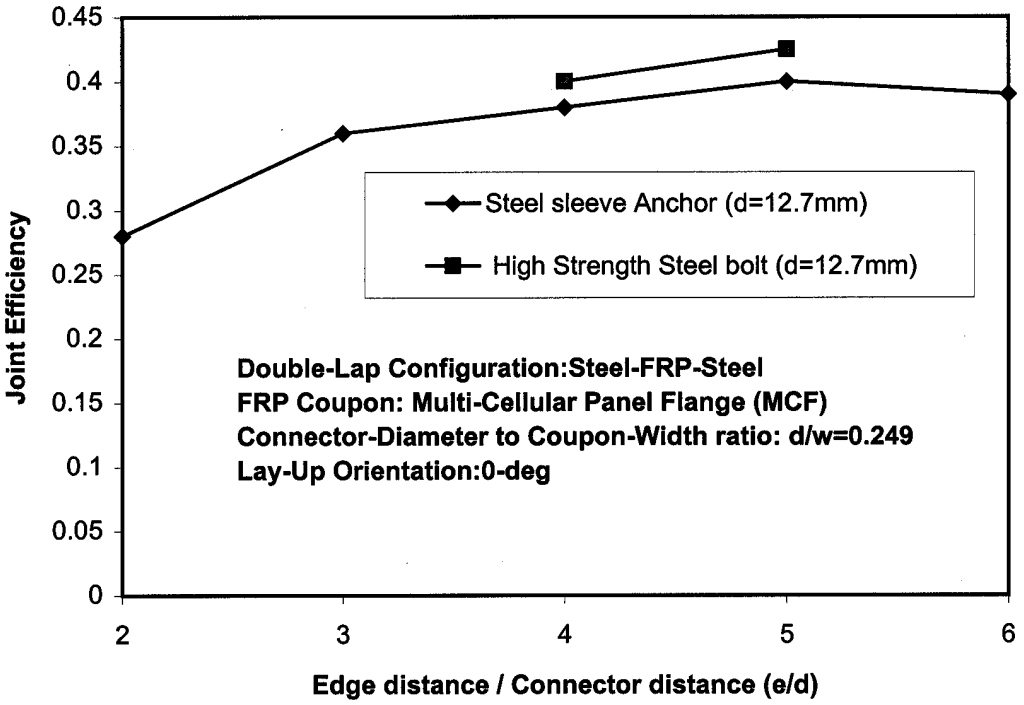

Figure 3.20. Joint efficiency with steel sleeve anchors and high-strength bolts.

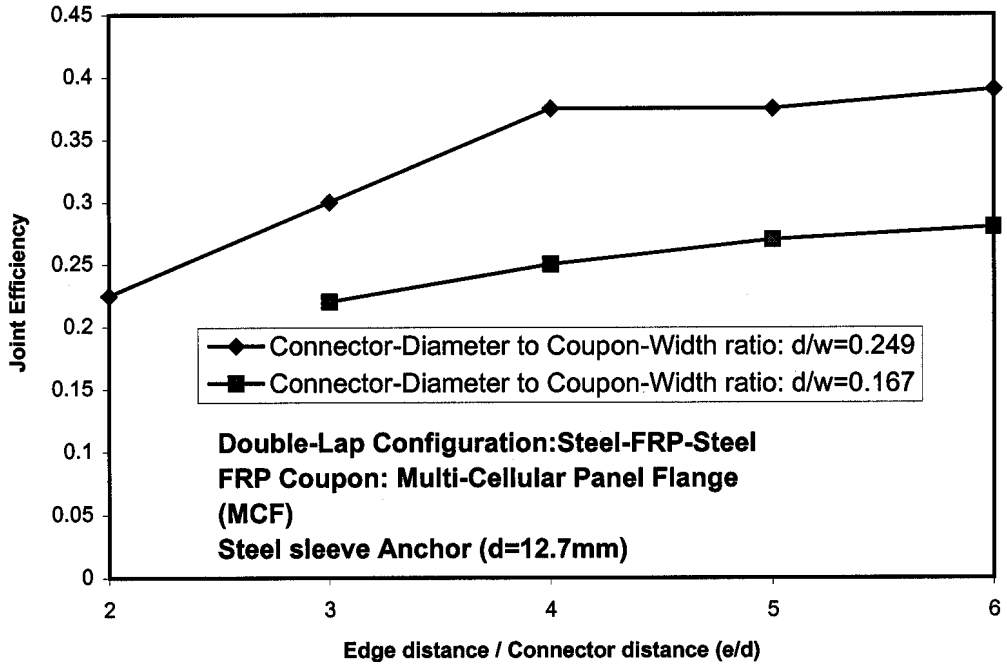

Figure 3.21. Joint efficiency for two-bolt-diameter-to-coupon width ratios.

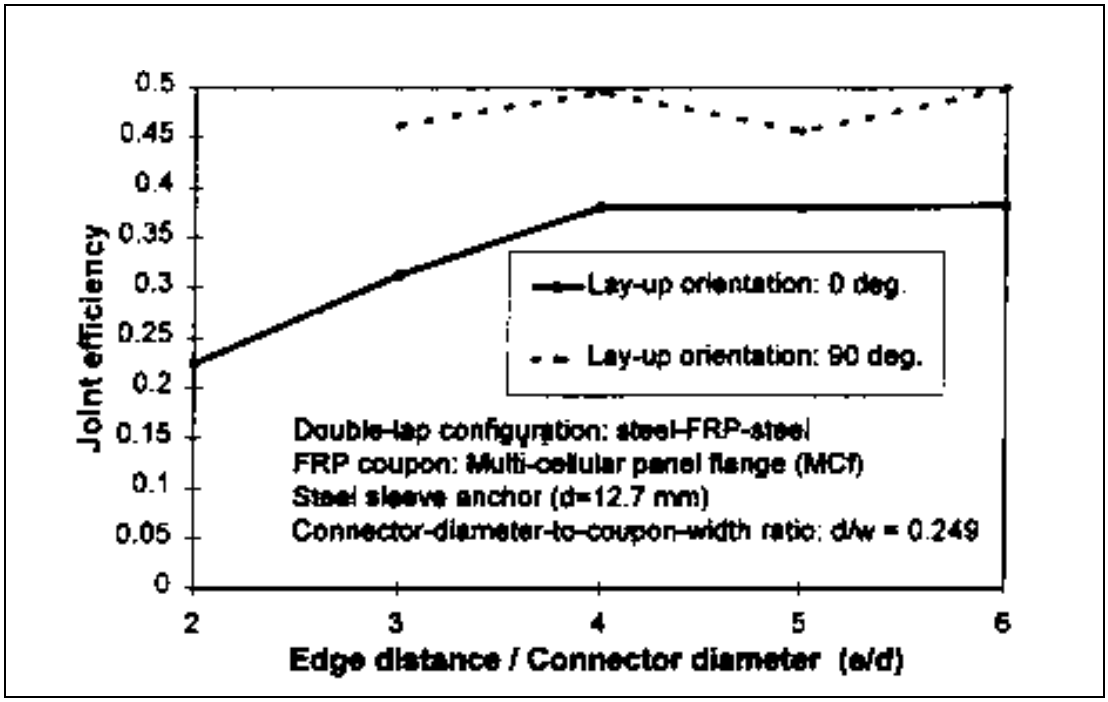

Figure 3.22. Joint efficiency for 0-degree and 90-degree lay-up orientation.

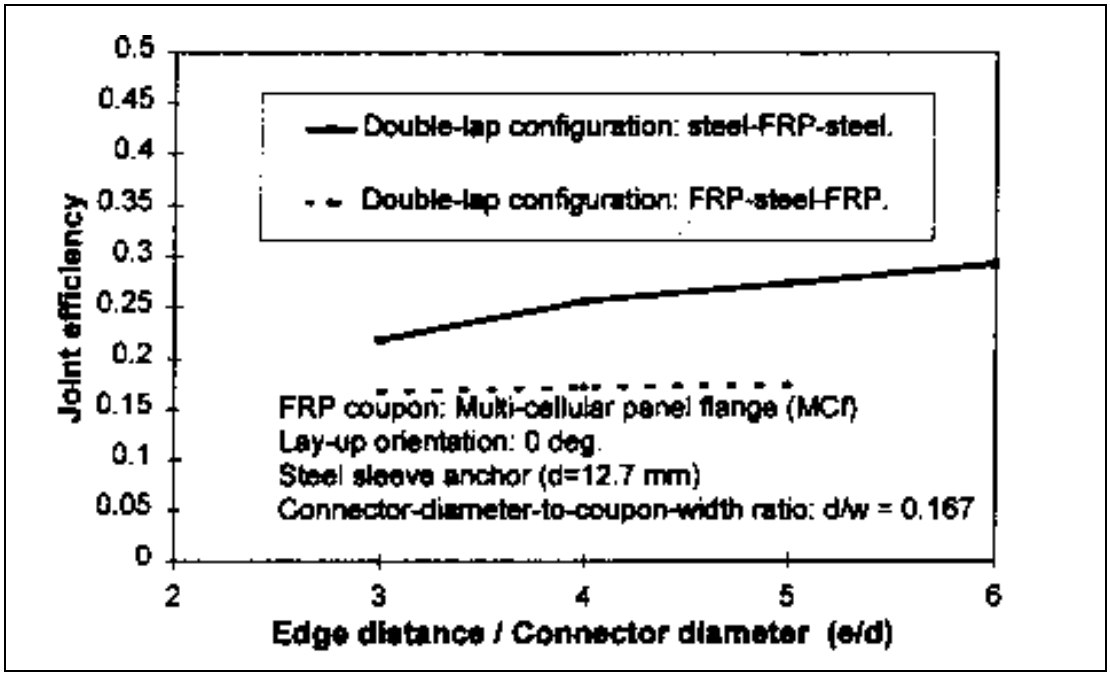

Figure 3.23. Joint efficiency for two steel-FRP double lap configurations.

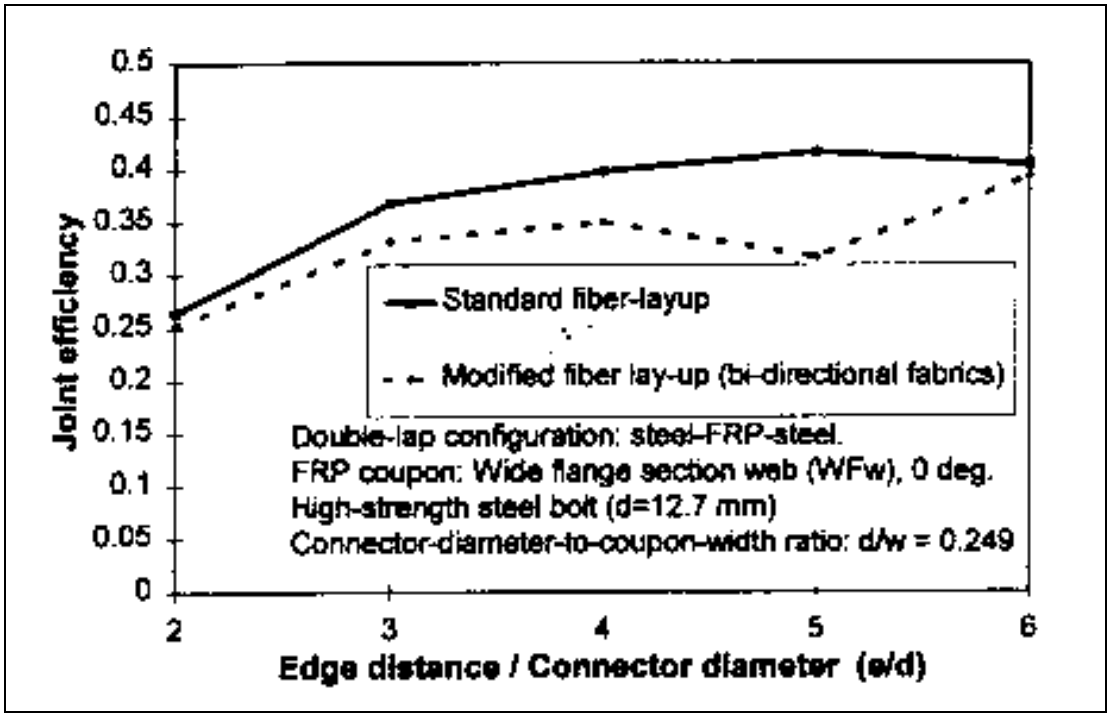

Figure 3.24. Joint efficiency for standard and modified fiber layout.

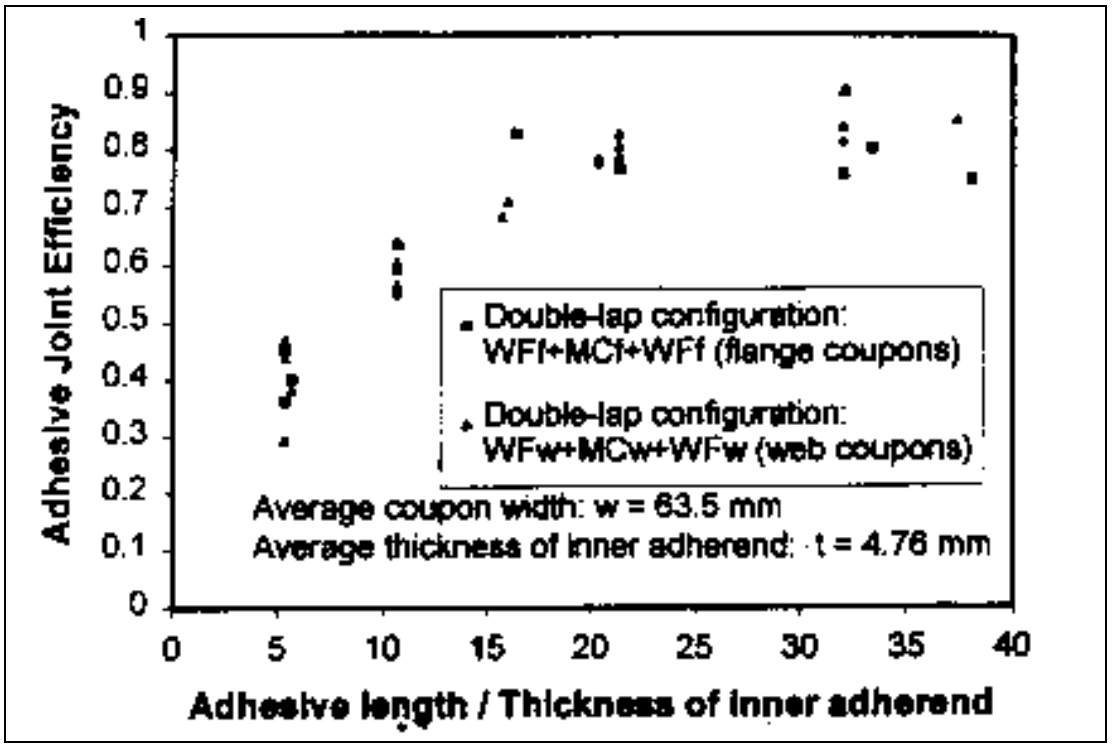

Figure 3.25. Joint efficiency of double lap adhesive joints.

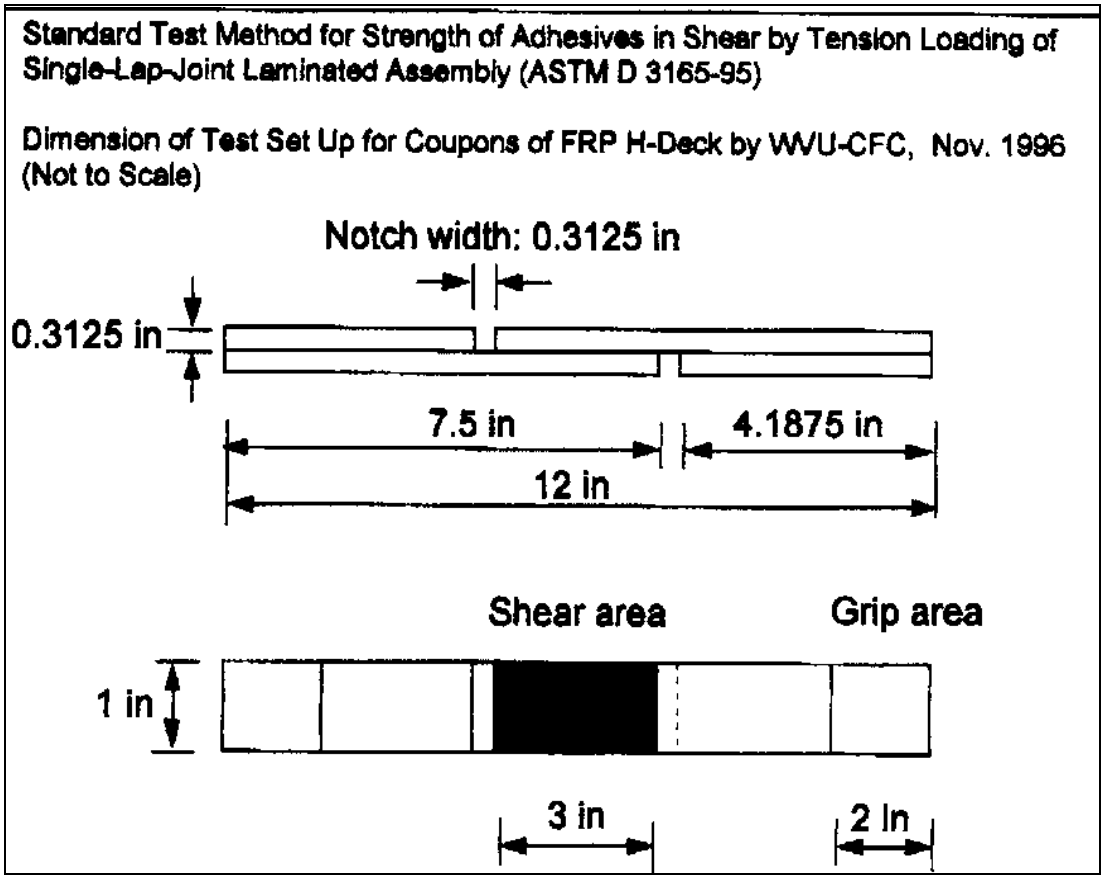

Figure 3.26. Setup and dimensions of single lap joint coupons for H-deck system.

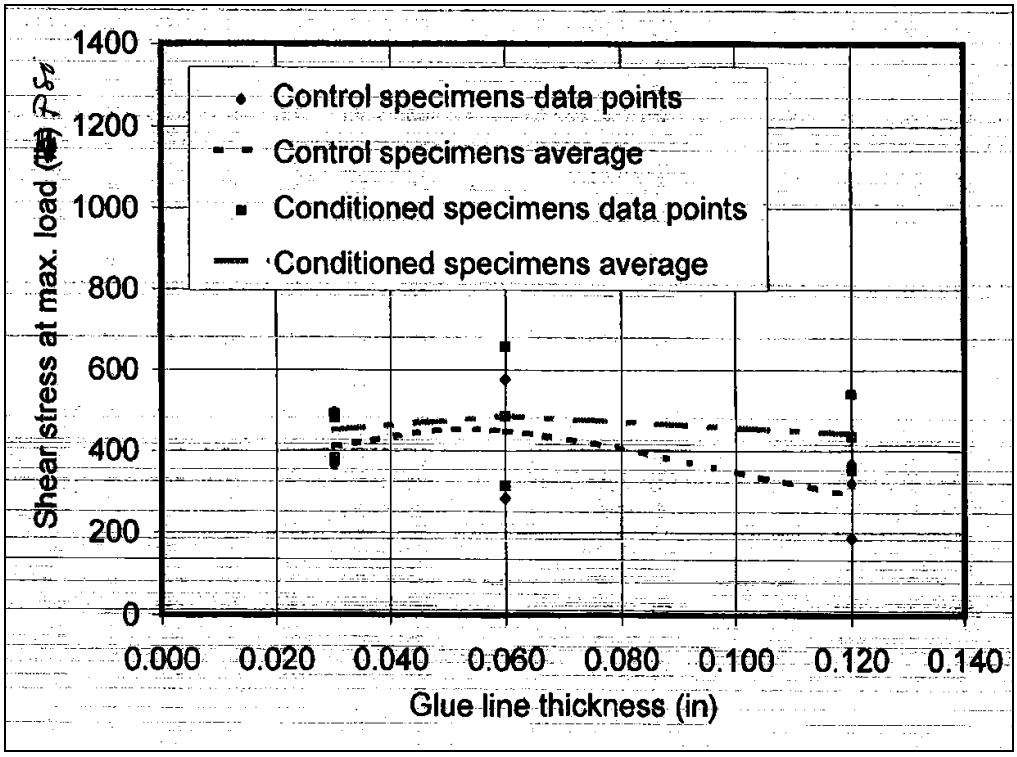

Figure 3.27. Strength of SIKADUR 30 adhesive in lap shear test.

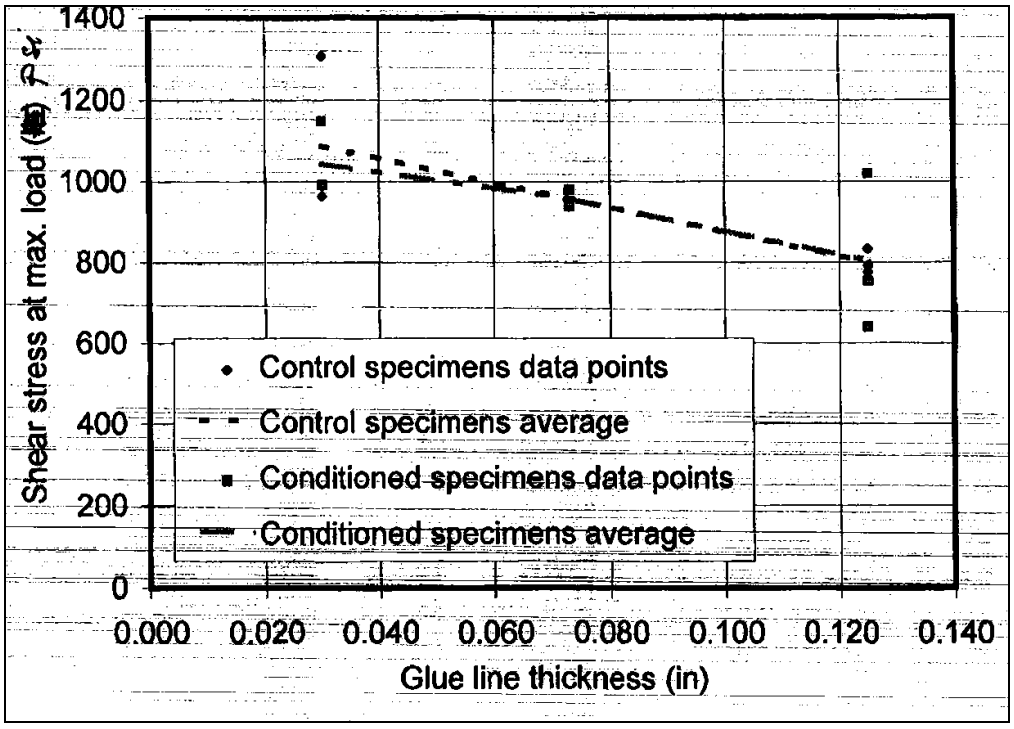

Figure 3.28. Strength of Pliogrip 6600/6600 adhesive in lap shear test.

Table 3.1. ANOVA of fatigue-deflection data to test correlation significance, VARTM H-Deck.

H-DECK 1

No. Cycles	LVDT 1	LVDT 2	LVDT 3	LVDT 4	LVDT 5	LVDT 6	LVDT 7	LVDT 8
0	0	0.278	0.420	0.288	0	0	0.274	0.402
500000	0	0.309	0.445	0.262	0	0		0.446
1000000	0	0.328	0.455	0.290	0	0		0.414
1500000	0	0.300	0.423	0.271	0	0		0.407
2000000	0	0.268	0.422	0.269	0	0	0.276	0.410

	LVDT 9	LVDT 10	LVDT 11	LVDT 12	LVDT 13	LVDT 14	LVDT 15
0	0.274	0	0.377	0.459	0.475	0.405	0.402
500000	0.300	0	0.453	0.505	0.513	0.411	0.415
1000000	0.287	0	0.506	0.511	0.445	0.432	0.445
1500000	0.284	0	0.513	0.485	0.414	0.415	0.398
2000000	0.283	0	0.523	0.482	0.409	0.411	0.389

Note: All LVDT deflections given in inches.

ANOVA

Source of Variation	*SS*	*df*	*MS*	*F*	*P-value*	*F crit*
Rows	0.002132	4	0.000533	0.247565	0.909954	2.536581

Table 3.2. ANOVA of fatigue-deflection data to test correlation significance, pultruded H-Deck.

H-DECK 3

No. Cycles	LVDT 1	LVDT 2	LVDT 3	LVDT 4	LVDT 5	LVDT 6	LVDT 7	LVDT 8
0	0	0.254	0.38	0.258	0	0.311	0.33	0.345
500000	0	0.249	0.369	0.256	0	0.309	0.334	0.346
1000000	0	0.247	0.364	0.253	0	0.306	0.332	0.344
1500000	0	0.247	0.364	0.254	0	0.309	0.334	0.345
2000000	0	0.246	0.361	0.251	0	0.308	0.334	0.345

	LVDT 9	LVDT 10	LVDT 11	LVDT 12	LVDT 13	LVDT 14	LVDT 15
0	0.385	0.404	0.392	0.353	0.324	0	0
500000	0.396	0.417	0.401	0.343	0.314	0	0
1000000	0.402	0.422	0.405	0.339	0.309	0	0
1500000	0.398	0.421	0.403	0.337	0.306	0	0
2000000	0.403	0.428	0.408	0.338	0.307	0	0

Note: All LVDT deflections given in inches.

ANOVA

Source of Variation	*SS*	*df*	*MS*	*F*	*P-value*	*F crit*
Rows	1.51E-05	4	3.77E-06	0.153592	0.960607	2.536581

4 Demonstration Projects

Introduction

In order to utilize and demonstrate the optimized FRP structural components developed under this project, two demonstration projects were identified. Both were short-span bridge applications on low-volume rural roads. The first bridge, constructed in May 1997, was the Laurel Lick Bridge, Lewis County, WV. For all practical purposes, this bridge is an all-composite structure consisting of pultruded FRP H-Deck modules, pultruded WF-FRP stringers and column/piles, and a thin polymer concrete wearing surface over the FRP deck. The second bridge, the Wickwire Run Bridge, Taylor County, WV, was constructed in July and August 1997. It consists of pultruded FRP hexagonal (H-Deck) modules on conventional steel stringers. The length and width of the Laurel Lick and Wickwire Run bridges are 20 ft by 16 ft, and 30 ft by 21.7 ft, respectively.

Laurel Lick Bridge

Design

A design standard for FRP bridges is not available, but the Laurel Lick Bridge was designed to meet the requirements for AASHTO HS 20 truck loads and comply with West Virginia Department of Highways criteria where applicable. The AASHTO LRFD Bridge Design Specification (1994) was used as the basis for the design criteria. The AASHTO design specification is based on the following:

$$(\text{load effects} \times \text{load factors}) \leq (\text{nominal strength} \times \text{resistance factor}) \quad \text{[Eq 4.1]}$$

The load effects (deformations, stresses, or stress resultants) and the corresponding load factors (e.g., dead load, vehicular load) were determined based on the AASHTO (1994) design specifications. Design details for the Laurel Lick Bridge are presented in Appendix B. Figure 4.1 is a section view of the bridge. The vehicular live load consisted of a standard design truck load, HS-20, and an impact load of 1.3 times the live load.

The nominal strength in Equation 4.1 is based on the deck dimensions as shown on the plans and on permissible stresses, strains, deformations, or specific strengths of the composite materials. The nominal strength is reduced by the resistance factors for strength limit state including factors for flexure, shear, compression, tension, and bearing. Furthermore, many of the structural systems have additional reduction factors that are unique to the specific structural application of the material, such as the tensile reduction factor to account for shear lag in structural steel connections (AASHTO 1994, p 6-41). Other parameters used in the establishment of resistance factors include manufacturing effects and time-dependent (aging) effects. The principal manufacturing variables are process repeatability, tooling quality, dimensional tolerances, curing control, void content, and fiber misalignment. The principal aging effects include chemical aging, moisture absorption, ultraviolet (UV) exposure and freeze thaw effects. Without a historical performance record for the time-dependent effects on FRP composite systems, very conservative assumptions are appropriate in selecting resistance factors for FRP composites. For example, in the design of the WF-FRP pile/columns, 0.25 was used as the resistance factor.

In the analysis of the bridge, superstructure deflection (not stress) was the controlling design criterion. Total bridge deflection under live load was limited to the bridge span divided by 500 (0.432 in. at midspan). As a result of the deflection control and the relatively low stiffness of the 12 in. x 12 in. x 1/2 in. WF-FRP stringers, the superstructure is not effective in utilizing its strength capacity.

Construction

The FRP structural elements and deck modules were fabricated by Creative Pultrusions, Inc. (Alum Bank, PA), and shipped to the bridge site. The deck was shipped in three modules (two 6 ft sections and one 7 ft section).

For the bridge substructure, WF-FRP columns, with an approximate length of 10 ft, transfer the vertical loads to a sandstone rock foundation. Five WF-FRP columns spaced 6 ft apart were installed in each abutment. After drilling the foundation to a depth of 5 ft, the FRP composite columns were placed and concrete was poured. Constructed multicellular FRP panels were used for lagging between the columns. The FRP columns were embedded in the reinforced concrete cap beam.

In the superstructure, the six 20 ft long WF-FRP beams were attached to the reinforced concrete cap beams with steel clip plates. The FRP deck modules

were connected to the FRP supporting beams using engineered 0.5 in. blind fasteners (BOM™ bolts) from Huck International, Inc. The blind fasteners includes a zinc plated carbon steel sleeve and an alloy steel core. A special hydraulic tool is used to apply a pulling force to the core, and this force expands the sleeve to provide the positive clamping required for the connection (Sotiropoulos, GangaRao, and Lopez-Anido 1996, pp 233-242).

In addition to the blind fasteners, a two-part polyurethane adhesive (PLIOGRIP® 6600) was used to bond the FRP deck to the FRP stringers and bond the splices of the deck modules together. Edge caps made of FRP flat sheets and angles were used to close the cells on both sides of the deck. Curbs were constructed with 5 in. FRP square-tube scupper blocks and continuous square tubes connected to the FRP deck. Figure 4.2 is a picture of superstructure under construction.

A thin polymer concrete overlay was applied on the FRP deck. The surface preparation of the deck included sandblasting, cleaning, and the application of a urethane-based primer to the FRP deck. Then polymer concrete was applied by the broom-and-seed method to an approximate 3/8 in thickness and overlaid with clean sand. The polymer concrete binder was an isophthalic unsaturated polyester resin. The resin and primer were supplied by Reichhold Chemicals, Inc., Research Triangle Park, NC.

Wickwire Run Bridge

The Wickwire Run Bridge was constructed with the FRP modular deck supported by four longitudinal steel stringers spaced 6 ft apart. The design was based on the results of the experimental performance validation of the H-Deck modules described in Chapter 3. The controlling issues include compliance with the AASHTO deck deflection limit (deck span divided by 300) and the HS 25 truck load.

The construction of the bridge was sequenced to have the placement of the deck to coincide with a field trip of the WVU Constructed Facilities Center meeting and group discussion on FRP materials. The actual field trip occurred during the afternoon of 29 July 1997. The FRP deck placement was observed by 48 people representing five state departments of transportation, the Federal Highway Administration (FHWA), bridge design consulting companies, the Army Corps of Engineers, and the Composites Institute.

Cost Benefit of FRP Composite Bridging

The cost-benefit analysis of the FRP composite shapes and the H-Deck system, based on bridge deck applications, indicates that the glass FRP composites beams and columns have excellent strength, but their low stiffness limits effective utilization of their high strength values. The H-Deck systems are less bothered by stiffness limits. They have real weight advantages over an equivalent thickness of concrete decking (22 lb per sq ft versus 100 lb per sq ft). Additionally, the H-Decks are prefabricated deck modules that should be attractive for rehabilitation of existing bridges for which it is essential to reduce time out of service due to construction. When compared with prefabricated concrete decks, the low weight of the composite H-Deck will allow for deck placement with a light backhoe bucket, as opposed to a heavier crane required for the placement of a prefabricated concrete deck. Based on the two demonstrations, it is estimated that a crew of four can place 75 sq ft of FRP deck per hour, as compared to about 30 sq ft of reinforced concrete deck per hour by the same size crew.

FRP-composite beams, even with their low stiffness, may have a market for use in bridges that are slightly longer than common prefabricated box culverts (i.e., 12 ft and under).

The H-Decks used in the demonstration bridges cost approximately $70 per sq ft. The manufacturer, Creative Pultrusions, Inc., intends to market the decks for approximately $50 per sq ft based on a version of the product redesigned by WVU–CFC. A complete concrete deck for the same applications would cost $30 to $40 per sq ft. If the FRP deck has a longer life and lower installation cost than reinforced concrete, as anticipated on the basis of decades of engineering experience with this material, the FRP composite H-Deck system will have a significant life-cycle cost advantage over conventional reinforced concrete decks.

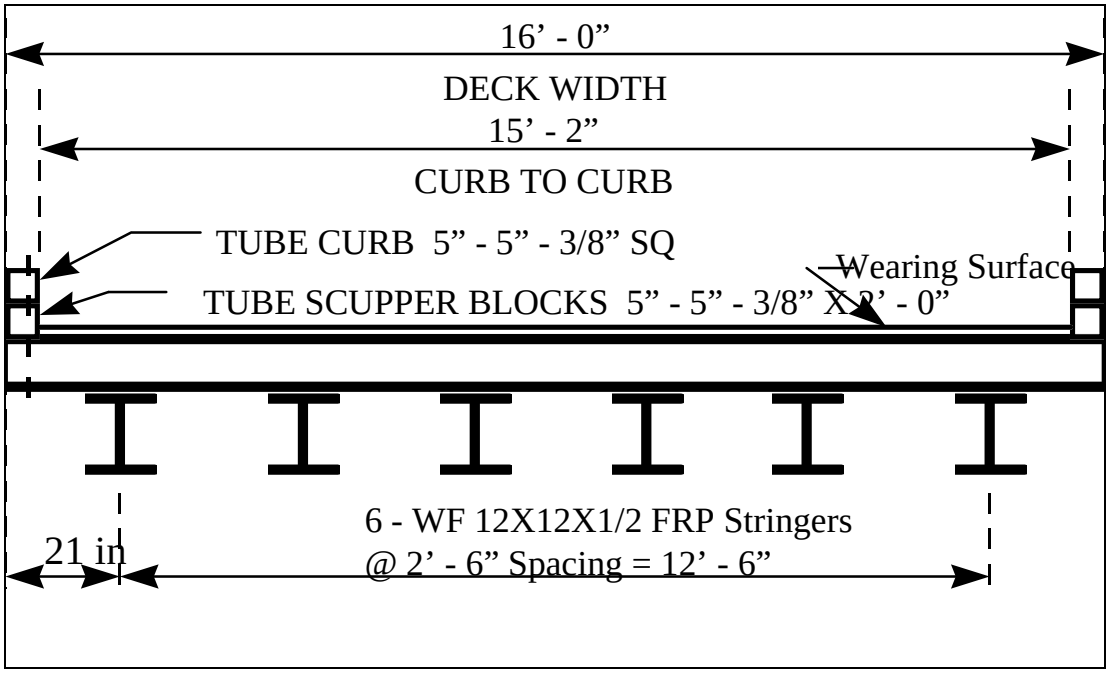

Figure 4.1. Deck section of Laurel Lick Bridge.

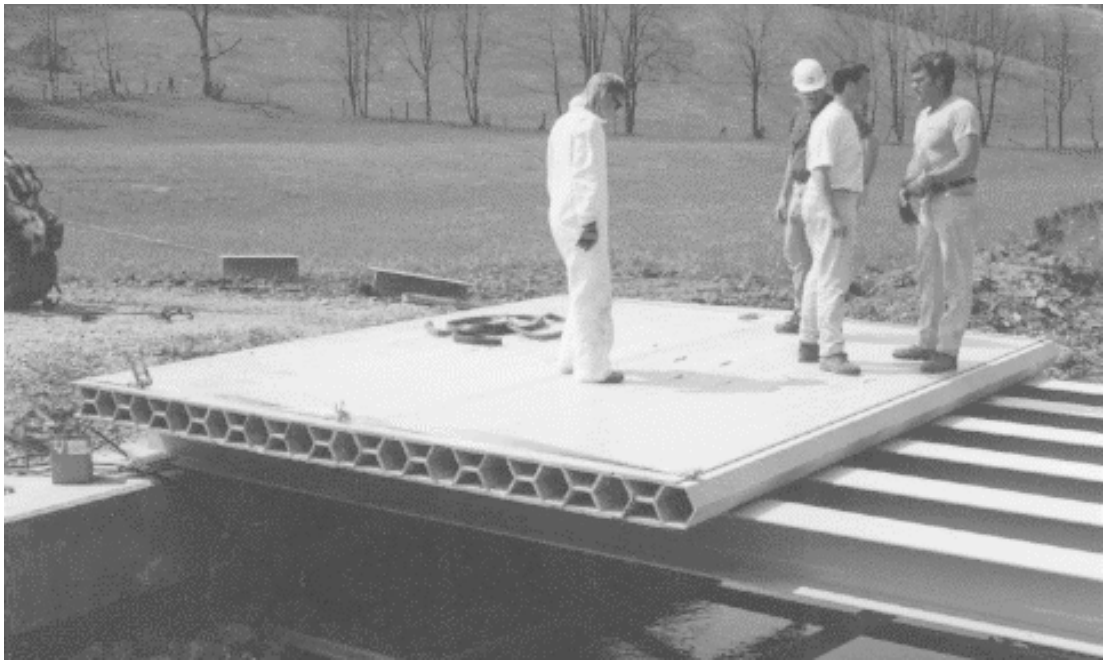

Figure 4.2. Placement of H-Deck sections on FRP stringers for Laurel Lick Bridge.

5 Conclusions, Recommendations, and Commercialization

Conclusions

This CPAR research effort succeeded in meeting the objectives defined in the CPAR Research, Development, and Commercialization Plan: to develop, test, and demonstrate optimized, advanced-design composite structural components for civil engineering applications, and to develop material standards, specifications, and design protocols for these advanced composite components.

From the results of the research the following conclusions are drawn:

1. Two new FRP composite fiber architectures were developed for 12 in. x 12 in. x 0.5 in. WF beams. The new fiber architectures, when compared to the off-the-shelf composite product, had a stiffness increase of 34 – 55 percent. Even with this new fiber architecture, however, deflection controlled the design of bridge stringers, thus limiting the efficiency of using the material's high strength capacity.

2. Two new FRP composite fiber architectures were developed for 12 in. x 12 in. x 0.5 in. WF columns. The average localized buckling strength of the two new fiber architectures were 37 and 63 percent higher than the local buckling strength of the off-the-shelf samples. Compression tests on short columns indicated that compressive stiffness is influenced by test temperature, with a 25 percent stiffness increase between 23 °C and -40 °C.

3. The shape and architecture of the hexagonal H-Deck system was optimized and tested. Additionally, a winged box beam and unicolumn were proposed, but these were not fabricated or tested due to the cost of creating new pultrusion dies. The tests on the H-Deck systems focused on stiffness, ultimate strength, and fatigue degradation. The simulated live load tire patch tests indicated that the deck systems — both the VARTM and pultruded versions — exceeded the AASHTO HS25 truck live load by a factor of 6 for the maximum 9 ft span. Additionally, at the 9 ft span, live load deck deflection did not exceed l/500. No

statistically significant fatigue degradation occurred in either deck system over 2 million load cycles.

4. Two demonstration bridges were successfully constructed using the composite H-Deck. The first bridge, constructed in May 1997, was the Laurel Lick Bridge, Lewis County, WV. The second bridge, the Wickwire Run Bridge, Taylor County, WV was constructed in July and August 1997. Both applications were short-span bridges on low volume local rural roads. The Laurel Lick Bridge was a complete FRP composite bridge, including composite stringers, pile columns, and H-Deck. The Wickwire Run Bridge was a composite H-Deck on steel stringers. The length and width of the Laurel Lick and Wickwire Run bridges are 20 ft x 16 ft and 30 ft x 21.7 ft, respectively.

5. A cost-benefit analysis of using FRP composite shapes and the FRP H-Deck system in bridge decks indicates that the glass FRP beams and columns have excellent strength, but their low stiffness limits effective use of their high strength values. The H-Deck systems, however, are less bothered by stiffness limits and they are much lighter than concrete decking of equal thickness. The H-Decks are prefabricated deck modules that should be attractive for rehabilitation of existing bridges where reducing downtime is critical. H-Decks for the demonstration bridges cost approximately $70 per sq ft (1997 price). The manufacturer (Creative Pultrusions, Inc., Alum Bank, PA) indicates that it intends to market the decks for approximately $50 per sq ft. The cost compares to $30 to $40 per sq ft for a complete concrete deck. If the FRP composite H-Deck has a longer life, as is anticipated, it will have a significant life-cycle cost advantage over conventional reinforced concrete decks.

Recommendations

It is recommended that the pultruded FRP H-Deck system be used in other decking applications for highway bridges. The initial cost for materials is higher than for conventional reinforced concrete decking, but the FRP H-Deck can be expected to offer a significant life-cycle cost benefit due to lower handling and installation costs and the elimination of corrosion problems. Also, the H-Deck system cost can be reduced further with modifications to the fiber/fabric architecture and further optimization in the manufacturing process. The FRP H-Deck is recommended for deck rehab-replacement applications where minimizing the bridge downtime and dead loads is critical. The prefabricated and relatively light deck modules will minimize the amount of time a bridge is out of service for the deck replacement.

The pultruded FRP composite beams and columns studied here may be recommended for a significant niche market in highway bridging: short-span rural bridges similar to the Laurel Lick demonstration bridge. Such bridges are at the upper end of prefabricated box culvert applications but short enough that deflection control is not a major impairment.

Beams, columns, and H-Decks could be refined for greater improvements in the efficiency of material use. It is recommended that a greater variety of sections be evaluated and tested. For example, a greater variety of beam sections — particularly deeper sections — would provide for greater stiffness and more efficient use of materials.

Additional testing of this technology is recommended. The objective of this testing would be to support proper identification of resistance factors for FRP composite structural systems in the ASSHTO LRFD design procedure. The testing conducted in this study was directed to assure compliance with project-specific design assumptions: further testing is now needed to identify the general performance envelop of these structural FRP composite systems.

It is recommended that efforts continue toward developing materials standards through ASTM and standard design procedures through ASCE and/or AASHTO.

Technology Transfer and Commercialization

Corps of Engineers Technology Transfer

Bridges are not a major component in the Corps Civil Works infrastructure or the Army's military facilities infrastructure. A recent inventory of public access bridges requiring Federally mandated safety inspections indicated that Civil Works has 259 public access vehicular bridges, and Army installations have approximately 1500. The Corps of Engineers — both in the Civil Works and Military Construction programs — relies on AASHTO for its bridge design criteria. Therefore, for the Corps to consider routine use of composite bridge systems, AASHTO would have to include resistance factors for composite decks and stringers in the Load and Resistance Factor Design.

WVU–CFC Technology Transfer Activities

In the area of standards and specifications, the Constructed Facilities Center (CFC) at West Virginia University (WVU–CFC) continues to work with the American Society of Civil Engineers (ASCE) and the American Society for

Testing and Materials (ASTM) to develop design procedures and specifications for FRP composite structural applications. Additionally, WVU–CFC participates in standards development as a member of the U.S. delegation to a joint U.S.-Canadian committee on standards for FRP structural composites.

WVU–CFC also continues to work with interested potential end users (West Virginia Department of Transportation and Pennsylvania Department of Transportation) and Creative Pultrusions, Inc., to enhance the material properties, ductility, and durability of the optimized FRP pultruded shapes. This effort includes interaction with the producers of constituent materials (i.e., fibers, fabrics, and resins) to improve manufacturing capability by improving wetability, minimizing fabric kinks and voids, and improving the sweep of the structural shapes produced in this work. Proposals are subject to the availability of funding support.

Other pending activities, subject to funding by interested future partners, include:

- development and publishing design guidelines and procedures for FRP shapes using first principles of materials mechanics
- presenting the results of developmental work at various technical conferences and interacting with key people, including governmental agencies and university personnel on the research results
- field monitoring of the two demonstration bridges for static and dynamic response and long-term durability.

WVU–CFC, in partnership with the West Virginia Department of Transportation – Division of Highways, will conduct performance monitoring of the two demonstration bridges for 3 years with funding provided by the U.S. Department of Transportation – Federal Highway Administration.

The pultrusion H-Deck is commercially available now from Creative Pultrusions, Inc., Alum Bank, PA, a CPAR partner participant in this research.

Composites Institute Market Development Alliance Activities

The CI/MDA has developed a pre-commercialization model that provides crosscutting mechanisms intended to accelerate the steps required to demonstrate and commercialize new FRP composite products. One CI technology transfer goal is to integrate the technical achievements from the present study into the CI Pultrusion Industry Council. Also, the CI will initiate industry

organizations and activities to carry out portions of the technology transfer plan. The CI/MDA plan comprises the following seven steps.

1. Initiate formation of composites industry councils

The CI/MDA has invited all interested FRP composites bridge suppliers to join a new industry group, the Composites Bridge Council. The council will provide engineers technical information on FRP composite structural materials and work with key trade-technical-and-professional organizations (TTPOs) in this area. Activities will include: publication of background information on composites; illustrated documentation of FRP composite construction applications, a construction practices handbook addressing handling, installation, M&R, etc.; manufacturers' product information; and a summary of expert resources.

The CI also plans to initiate another group, the Advanced Fiber Architecture Council in which material suppliers from the glass industry can work together to produce constituent products (e.g., bridge decks) that can be used in the fabrication of products used for the civil infrastructure.

2. Establish Technology Transfer Advisory Board

This board would provide input during the development process to ensure that basic technical decisions about new products consider real-world issues important to all stakeholders in the construction marketplace. The board may include architects, designers, structural engineers, contractors, TTPOs, code bodies, and regulatory organizations. Board input to FRP bridge suppliers would include the following:

- characterization of traditional materials and construction practices (strengths, weaknesses, needs, and industry influence factors)
- identification of performance-based specifications for various applications
- identification of installed-cost targets
- guidance in the development of standards and other regulatory approvals
- recommendation and coordination of new demonstration projects.

Board members also would provide liaison with bodies that may influence development of the industry and would advocate the technology within their respective professional communities.

3. Develop industry-level construction documents and preliminary standards

A critical technology transfer step is the development of construction documentation (means and methods), preliminary specifications and standards that represent recommended industry practice and lead to approval of developed products. This might be accomplished by engaging the Civil Engineering Research Foundation's new Civil Engineering Innovative Technology Evaluation Center (CE-ITEC) to design an evaluation and testing program for the Concrete Bridge Council. Expected feedback from CE-ITEC would identify opportunities for product improvement and required modifications of practice, providing continual input into the research and development process. This activity falls beyond the scope and timing of the present CPAR study.

4. More demonstrations

Assuming that the evaluation process described above validates the product, widespread demonstration of the technology — focused on the prospective target market — will be promoted by the CI/MDA. Generally speaking, the number of field demonstrations will be directly proportional to the size of the target market and the number of suppliers offering the technology. Regional demonstrations can be organized in conjunction with the Technology Transfer Advisory board and participating TTPOs.

5. Continuing Promotion and Publicity

Promotional activity will be targeted at the engineering community. Case histories will be publicized in construction journals and magazines such as *Engineering News Record*, *Roads & Bridges*, and the *Journal of Composites for Construction*. Whenever possible, demonstration sites will be used for promotional activities such as tours for local chapters of participating TTPOs.

6. Education and Training

Education and training materials will be created in cooperation with key construction industry TTPOs and publicized in industry publications. Another possible medium for disseminating education and training materials would be the World Wide Web (e.g., via CE-Net).

Workshops may be offered by CI at events such as the International Composites Exposition, or may be planned for traditional construction gatherings such as the annual ASCE conference and the International Bridge Conference. Plans in-

clude presentation of technical papers at every major industry event that discusses the present CPAR demonstration.

7. Continuing Commercial Proliferation

The steps discussed above are the essential elements of a full-scale commercial launch. The probability of successful commercial proliferation will be strongly enhanced when the technology transfer plan described above succeeds in integrating the development of FRP composites into the mainstream of the existing construction industry.

References

American Association of State Highway and Transportation Officials, "LRFD Bridge Design Specification" (Washington DC, 1994), pp 6-41.

Barbero, E. J., *Pultruded Structural Shapes: From the Constituents to the Structural Behavior,* SAMPE J., 27(1):25-30, 1991.

Civil Engineering Research Foundation, *Materials for Tomorrow's Infrastructure,* CERF Report #94-5011, Washington D.C. (December 1994), pp 49-50.

Jones, R. M., *Mechanics of Composite Materials* (Scripta Book Co., Washington. D.C., 1975).

Lopez-Anido, R., Hota V.S. GangaRao, M. Al-Megdad, and R. Bendidi, *Optimized Design of Fiber Architecture for Pultruded Beams,* Proceedings of Composites Institute's 51 Annual Conference, Paper 20-D (1996).

Lopez-Anido, R., R. Bendidi, H. V. S. GangaRao, M. Al-Megdad, *Local Buckling Experiments on Pultruded Composite Beams,* Proc. 4th Materials Engineering Conference, ASCE, pp 914-923 (1996).

Introduction to Composites, 3d ed. (Society of the Plastics Industry [SPI], Composites Institute, January 1995).

Sotiropoulos, S., and H. GangaRao, and R. Lopez-Anido, *Evaluation of FRP Composite Bolted and Adhesive Joints,* Proc. 4th Materials Engineering Conference, ASCE, pp 233-242 (1996).

Southwell, R., *Theory of Elasticity* (Oxford University Press, London, 1941).

Tomblin, J., E. Barbero, "Local Buckling Experiments on FRP Columns," *Thin Walled Structures,* 18, pp 97-116, 1994.

Tsai, S.W., *Structural Behavior of Composite Materials,* NASA CR-71 (National Aeronautics and Space Administration, July 1964).

Tsai, S.W., and H. T. Hahn, *Introduction to Composite Materials* (Technmonic Publishing Co., Lancaster, PA, 1980).

Appendix A: Test Series Design for Fatigue Study

This appendix provides details for the fatigue loads and truck tire patch dimensions used in the fatigue test series discussed in Chapter 3 of this report. Calculations were made per AASHTO LRFD Specification (1994).

Eq 6.6.1.2.2-1	$\gamma\Delta f < (\Delta F)_n$	(General limit state design criteria, p6-18)
Eq 1.3.2.1-1	$\eta\gamma(LL + IM) < \phi R_n$	(Design criteria for load-induced fatigue limit state, p 1-3)
Load factor	$\gamma = 0.75$	(Table 3.4.1-1, p 3-10)
Ductility Factor	$\eta_D = 1.00$	(Non-ductile; Article 1.3.3, p 1-4))
Redundancy Factor	$\eta_R = 1$	(Failure criteria; Article 1.3.4, p 1-5, 6)
Operational Importance Factor	$\eta_I = 1$	(Article 1.3.5, p 1-6)
Eq 1.3.2.1-2	$\eta = \eta_D * \eta_R * \eta_I$	η =1 (p 1-3)
Impact for Deck Joints	IM = 0.75 LL	(Table 3.6.2.1-1, p 3-27)

Fatigue Load = $\eta\gamma(LL + IM)$ = 0.75 * LL* (1 + .75) = 1.31 * LL

Multiple Presence Factor	MPF = 1	(Table 3.6.1.1.2-1, p 3-16)

LL = 16 kips for HS20 design truck wheel load (p 3-21)

Fatigue load for HS20 design truck = 1.31 * 16 = 21 kips

Deck width modification (effective deck width = ½ simply supported deck span)

Deck span (9 ft)	108 in.
Effective deck width	54 in.

Actual deck width and ratio:

VARTM	45 in.	0.83 ratio of effective width
Pultrusion	36 in.	0.67 ratio of effective width

Fatigue loads reduced for deck section widths:

VARTM	21 * 0.83 = 17.43 kips
Pultrusion	21 * 0.67 = 14.07 kips

Design fatigue requirement:

Average daily traffic (ADT) = 4000 (Max ADT = 20,000)

Average daily truck traffic (ADTT) = 20% of ADT, rural interstate (Table 3.6.1.4.2-1, p 3-25)

ADTT = 800 Assume two lanes, P = 0.85 (Table 3.6.1.4.2-1, p 3-25)

Eq 3.6.1.4.2-1 $ADTT_{SL}$ = ADTT * P = 680 (p 3-25)

Fatigue Design Life = 50 yr

Fatigue cycles for design life (assume two-lane bridge, an ADTT = 800, and two axles per truck) = 50 yr * 365 day/yr * 680 trucks/day * 2 axles/truck = 24,820,000 cycles @ 21 kips per cycle.

Fatigue load required for equivalent degradation in a 2,000,000 cycle experiment: assume a log-log fatigue life load relationship with a negative slope of three such that $N_{bridge} = N_{exp} * (dP_{exp}/dP_{Bridge})^3$ (based on load-fatigue life data for bridge steels).

Eq 6.6.1.2.5-1 Load conversion factor for equivalent degradation $(N_{bridge/} N_{exp})^{1/3}$ (p 6-27)

$(24,820,000/2,000,000)^{1/3} = 2.32$

Design fatigue load range for experimental setup:

VARTM	17.43 * 2.32 = 40.4 kips
Pultrusion	14.07 * 2.32 = 32.6 kips

Actual fatigue load settings for tests:

VARTM	Range 45 kips	Max 50 kips	Min 5 kips
Pultrusion	Range 33 kips	Max 35 kips	Min 2 kips

Truck tire length = 20 in. parallel to truck axis

Eq 3.6.1.2.5-1 Truck tire width = $Y(1+IM/100)P/2.5$ (p 3-22)

where

Y = load factor = Assume service I (deflection control) = 1 (Table 3.4.1-1, p 3-10)

IM = Impact factor = Assume deck joints - all limit state = 50%

P = wheel load for HS20 = 16 kips

Truck tire width = 1(1 + 0.5)(16/2.5) = 9.6 in. $\approx$ use 10 in.

Appendix B: Design Summaries of Two CPAR Demonstration Bridges

Laurel Lick Bridge

Superstructure

Finite element analysis was used to design and analyze the bridge stringer and deck system. Figure B.1 is a cross-section of the bridge stringer and deck system, including the location of the wheel loads. The geometry and materials properties outlined in Table B.1 were used in the finite element analysis. The deck was modeled using orthotropic shell elements (bending and membrane stiffness) and the beams were modeled using line elements. Rigid links were used to connect the decks and the beams. The rigid links were set up to model both composite and non-composite action. The term composite action, as used here, means that shear transfer occurs between deck and stringer elements that are loaded in bending. Non-composite action here means that no shear transfer takes place between those elements when loaded in bending.

Stiffness was the controlling criterion in the Laurel Lick Bridge design. The design was controlled by limiting live load deflection to L/500 (0.432 in.). The design load was taken as an AASHTO HS20-44 truck. For worst-case deflections, the single axle was located at midspan with wheel loads placed 24 in. from the 9 in. curb (as illustrated in Figure B.1), and a 1.3 live load impact factor was used.

Finite element analysis for composite and non-composite action was conducted on both HS20 and HS25 design loads with and without the 1.3 impact factor. Table B.2 summarizes the midspan live load deflection of the beams for the four loading environments. Additionally, midspan deflections were computed for dead load and dead load plus live load for both the composite and non-composite action. Table B.3 summarizes the midspan dead load plus live load deflections for the HS20 and HS25 design loads.

A review of Tables B.2 and B.3 indicates that the L/500 deflection criterion is satisfied only with the HS20 live load without the impact factor, and assuming composite action.

Substructure

Wide flange FRP piles/columns with an approximate length of 10 ft transfer the vertical loads to the sandstone rock foundation. Five wide-flange columns spaced 6 ft apart were installed in each abutment. After drilling the foundation to a depth of 5 ft, the composite piles/columns were placed and concrete was poured. FRP multicellular panels were used for lagging between the columns. The FRP columns were embedded in the reinforced concrete cap beam. Table B.4 presents the design computations for the bridge substructure. These computations follow the AASHTO LRFD criteria with a conservative (0.25) estimate for the material reduction factor.

Wickwire Run Bridge

The superstructure of the Wickwire Run Bridge consisted of an FRP composite H-Deck on four conventional steel stringers with 6 ft center-to-center spacing (Figure B.2). Finite element analysis was used to design the bridge stringers and deck stringers in the same manner described for the Laurel Lick Bridge superstructure. Stiffness was the controlling design criterion, and the midspan deflections were determined both for composite and non-composite action. The design load was taken to be the AASHTO HS20-44 truck. Two load cases are depicted in Figures B.3 and B.4: one asymmetric truck (Load Case 1) and two symmetric trucks (Load Case 2), respectively. Table B.5 summarizes the midspan live load plus impact load for Load Case 1, and Table B.6 summarizes the midspan live load plus impact load for Load Case 2.

A review of Tables B.5 and B.6 indicates that the L/500 (0.72 in.) deflection criterion was satisfied by the live load with the 1.3 impact factor added in all load cases.

Table B.1. Properties of composite deck and beam sections.

Deck Properties		Beam Properties	
Width	= 16 ft	Length	= 18 ft
Length	= 18 ft	Spacing	= 30 in
Thickness	= 8 in	Area	= 5.75 in^2
EI_x	= 2.15E9 in	Depth	= 12 in
Ei_y	= EI_x/10	Flange width	= 12 in
Poisson Ratio	= 0.25	I_x	= 468.78 in^4
Weight	= 22 lb/ft^2	I_y	= 144 in^4
Wearing Surface Weight*.	= 25 lb/ft^2	I_z	= 0.2 * I_x
(*) Wearing surface weight (WVDOT specified)		E_x	= 4.59E6 psi
		E_y	= 4.40E6 psi
		Poisson ratio	= 0.25
		Weight	= 15 lb/ft or 5.625 lb/ft^2

Table B.2. Midspan beam deflections for HS20 and HS25 loads for composite and non-composite action.

Non-Composite Action						
Beam	**X coord**	**HS20**		**HS25**		**TLDF**
	in.	16 kips	1.3×16 kips	20 kips	1.3×20 kips	
B1	21	0.621	0.807	0.776	1.009	0.232
B2	51	0.530	0.688	0.662	0.861	0.198
B3	81	0.458	0.595	0.572	0.744	0.171
B4	111	0.402	0.522	0.502	0.653	0.150
B5	141	0.353	0.459	0.441	0.573	0.132
B6	171	0.318	0414	0.398	0.517	0.119
Composite Action						
Beam	**X coord**	**HS20**		**HS25**		**TLDF**
	in.	16 kips	1.3×16 kips	20 kips	1.3×20 kips	
B1	21	0.378	0.492	0.473	0.615	0.237
B2	51	0.322	0.418	0.402	0.523	0.202
B3	81	0.277	0.360	0.346	0.450	0.174
B4	111	0.239	0.311	0.299	0.389	0.150
B5	141	0.203	0.264	0.254	0.330	0.128
B6	171	0.174	0.227	0.218	0.283	0.109

Table B.3. Midspan beam deflections computed with finite element model for dead load plus HS20 and HS25 live loads for composite and non-composite action.

Non-Composite Action						
Beams	**X coord in.**	**DL in.**	**HS20 in.**	**HS20+DL in.**	**HS25 in.**	**HS25+DL in.**
B1	21	0.144	0.621	0.765	0.776	0.920
B2	51	0.133	0.530	0.663	0.662	0.795
B3	81	0.128	0.458	0.586	0.572	0.700
B4	111	0.128	0.402	0.530	0.502	0.630
B5	141	0.133	0.353	0.486	0.441	0.574
B6	171	0.144	0.318	0.462	0.398	0.542
Composite Action						
Beams	**X coord in.**	**DL in.**	**HS20 in.**	**HS20+DL in.**	**HS25 in.**	**HS25+DL in.**
B1	21	0.085	0.378	0.463	0.473	0.558
B2	51	0.079	0.322	0.401	0.402	0.481
B3	81	0.076	0.277	0.353	0.346	0.422
B4	111	0.076	0.239	0.315	0.299	0.375
B5	141	0.079	0.203	0.282	0.254	0.333
B6	171	0.085	0.174	0.259	0.218	0.303

Table B.4. FRP column/piles for the bridge abutments.

FRP column sections fiber architecture			**Dead load computation = Dead Load per unit area**	
WF 12x12x1/2 A2 (Optimized for columns)			Wearing surface + Deck + FRP Beams 25 + 22+ 5.625 = 52.625 lb/ft^2	
Dead Load Resultant on Column				
Superstructure				
Length (ft)	Width (ft)	Area (ft^2)	Total wt (lb)	Wt per Abutment (lb)
20	16	320	16840	8420
Column Cap (Reinforced Concrete)				
Width (ft)	Height (ft)	Length (ft)	Unit Wt (lb/ft^3)	Abutment Wt (lb)
3	2	28	150	25200
Total Abutment Resultant (Superstructure + Column Cap) = 33620 lb				
Dead Load per column (Total Abutment Resultant/number of columns) = 6724 lb				
Live Load Computation (HS25 design Truck load with impact)				
HS25 Wheel load (lb)		Impact factor		Wheel load + Impact
20,000		1.3		26,000 lb
Load Combinations (Live load $\times$ LL factor + Dead Load $\times$ DL factor) 26,000 $\times$ 1.75 + 6,724 $\times$ 1.25 = **53,905** lb				
Load Capacity of Column Load capacity of FRP column is based on local buckling capacity. Local buckling for WF 12$\times$12$\times$1/2 with A2 fiber architecture was obtained experimentally, as described in Chapter 2 of this report. Material reduction factor is assumed to be 0.25 (accounting for material aging)				
WF Local Buckling (lb)		Material Reduction Factor		Design Strength (lb)
260,000		0.25		**65,000**
Design Strength is greater than Factored Load OK				

Table B.5. Midspan beam deflections for Load Case 1 (HS20 + impact) for composite and non-composite action on Wickwire Run Bridge.

Non-Composite Action			
		HS20	
Beam	**X coordinate (in.)**	**16 kips (in.)**	**1.3*16 kips (in.)**
B1	22	0.137	0.178
B2	94	0.154	0.200
B3	166	0.104	0.135
B4	238	0.021	0.027

Composite Action			
		HS20	
Beam	**X coordinate (in.)**	**16 kips (in.)**	**1.3*16 kips (in.)**
B1	22	0.086	0.112
B2	94	0.092	0.120
B3	166	0.064	0.083
B4	238	0.030	0.039

Table B.6. Midspan beam deflections for load case 2 (HS20 + impact) for composite and non-composite action on Wickwire Run Bridge.

Non-Composite Action			
		HS20	
Beam	X coordinate (in.)	16 kips (in.)	1.3*16 kips (in.)
B1	22	0.194	0.252
B2	94	0.227	0.295
B3	166	0.227	0.295
B4	238	0.194	0.252

Composite Action			
		HS20	
Beam	X coordinate (in.)	16 kips (in.)	1.3*16 kips (in.)
B1	22	0.130	0.169
B2	94	0.143	0.186
B3	166	0.143	0.186
B4	238	0.130	0.169

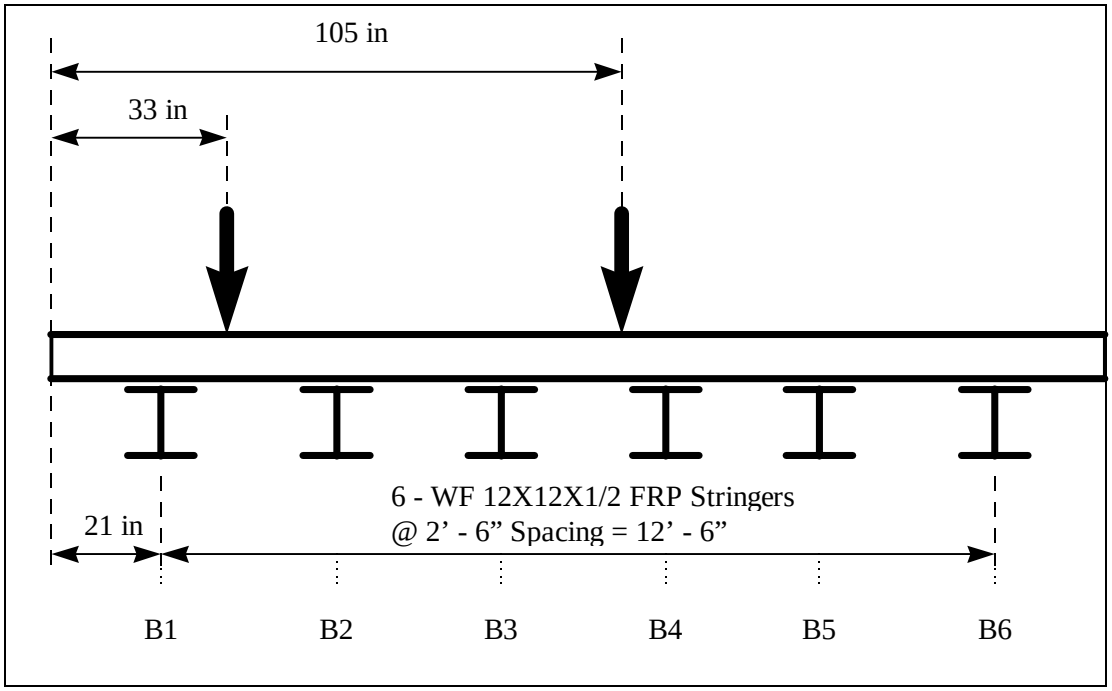

Figure B.1. Laurel Lick Bridge cross-section and location of wheel loads.

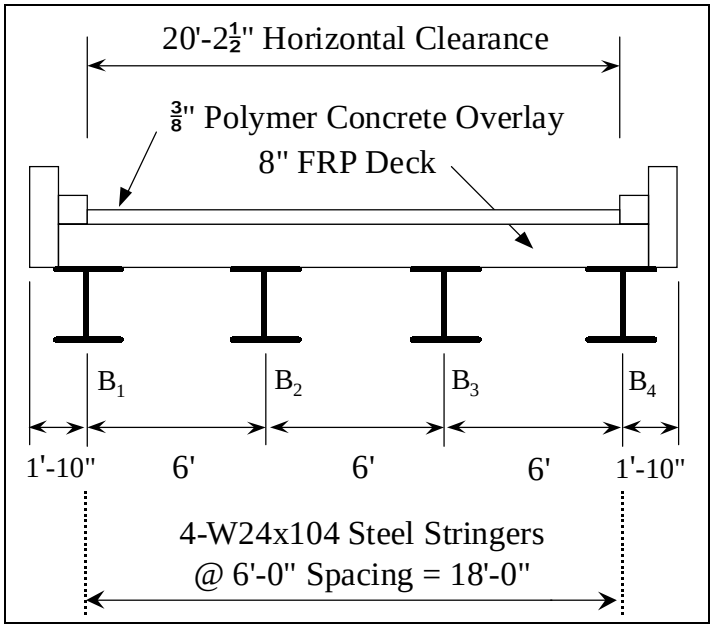

Figure B.2. Wickwire Run Bridge deck cross section.

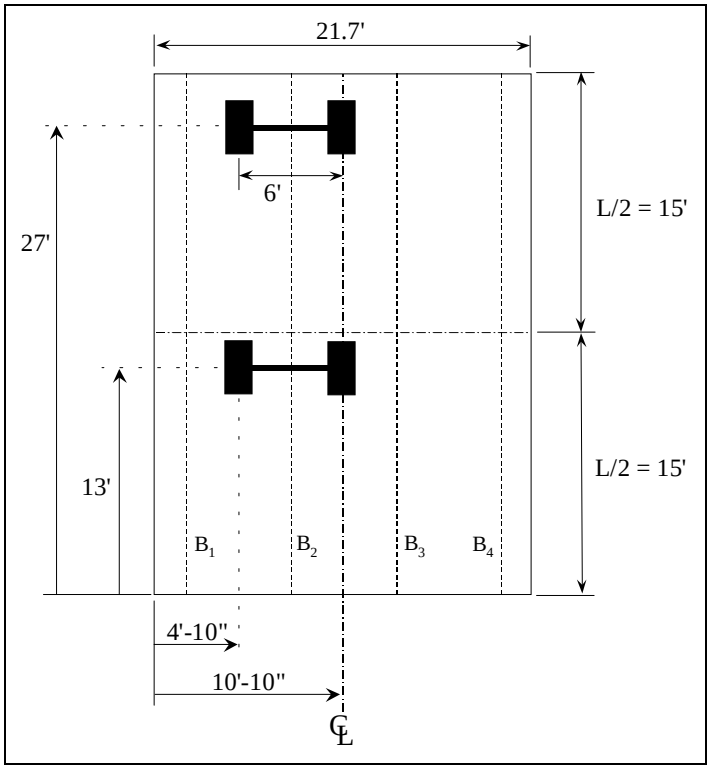

Figure B.3. Load case 1 — one asymmetric truck, Wickwire Run Bridge.

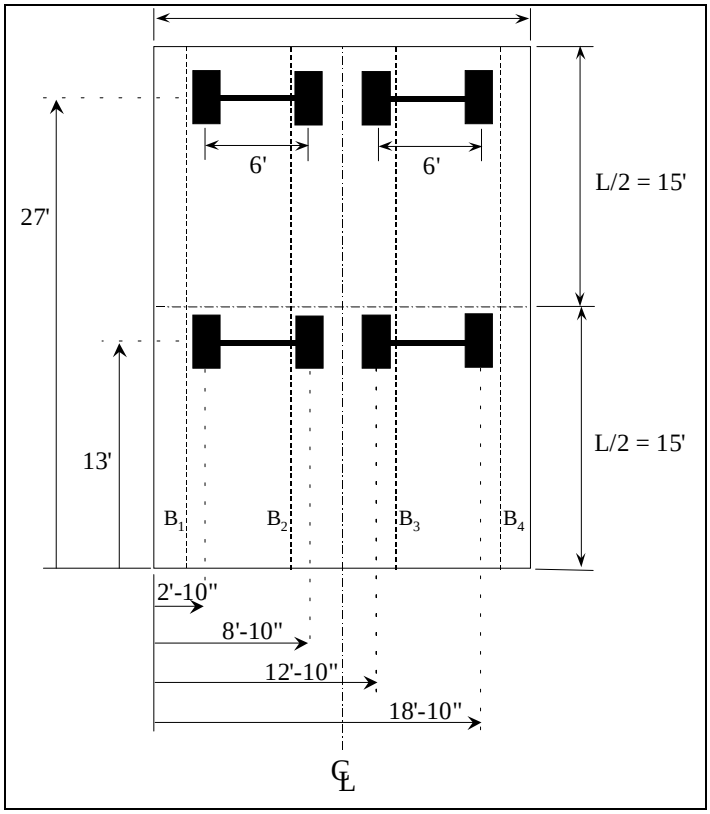

Figure B.4. Load case 2 — two symmetric trucks, Wickwire Run Bridge.

USACERL DISTRIBUTION

Chief of Engineers
ATTN: CECW-ED
ATTN: CEHEC-IM-LH (2)
ATTN: CEHEC-IM-LP (2)
ATTN: CEMP-CE
ATTN: CEMP-ET
ATTN: CERD-C (2)

US Army Engineer District
ATTN: Library (40)

US Army Engineer Divisions
ATTN: Library (11)

Defense Tech Info Center 22304
ATTN: DTIC-O (2)

62
+50
11/97